EUROPEAN RESPIRATORY journal
OFFICIAL SCIENTIFIC JOURNAL OF THE ERS

Prognostic phenotypes of early-stage lung adenocarcinoma

Journal:	*European Respiratory Journal*
Manuscript ID	ERJ-01674-2021.R1
Manuscript Type:	Original Research Article
Date Submitted by the Author:	30-Oct-2021
Complete List of Authors:	Lamort, Anne; Comprehensive Pneumology Center (CPC) and Institute for Lung Biology and Disease (iLBD); Ludwig-Maximilians University and Helmholtz Center Munich, Member of the German Center for Lung Research (DZL), Kaiser, Jan-Christian; Helmholtz Zentrum Munchen Deutsches Forschungszentrum fur Umwelt und Gesundheit, Institute of Radiation Medicine PEPE, Mario; Helmholtz Zentrum Munchen Deutsches Forschungszentrum fur Gesundheit und Umwelt Lilis, Ioannis Taliarda, N; University of Patras, Laboratory for Molecular Respiratory Carcinogenesis, Department of Physiology, Faculty of Medicine Somogyi, Kalman; German Center for Lung Research; German Cancer Research Center (DKFZ), Division of Molecular Thoracic Oncology Spella, Magda; School of Medicine, University of Patras , Department of Physiology Behrend, Sabine; Helmholtz Center Munich German Research Center for Environmental Health Giotopoulou, Georgia; Helmholtz Zentrum Munchen Deutsches Forschungszentrum fur Gesundheit und Umwelt, Comprehensive Pneumology Center (CPC) and Institute for Lung Biology and Disease (iLBD); Helmholz Zentrum Munich Kujawa, Willem; Helmholtz Zentrum Munchen Deutsches Forschungszentrum fur Gesundheit und Umwelt Lindner, Michael; Ludwig-Maximilian-University of Munich and Asklepios Medical Center, Center for Thoracic Surgery Munich Koch, Ina; Comprehensive Pneumology Center, Ludwig-Maximilians-University, University Hospital Grosshadern, and Helmholtz Zentrum München, Hatz, Rudolf; Ludwig-Maximilian-University of Munich and Asklepios Medical Center, Center for Thoracic Surgery Munich Behr, Jürgen; University of Munich, Campus Grosshadern, Munich, Germany, Department of Internal Medicine V, Comprehensive Pneumology Center, Member of the German Center for Lung Research Sotillo, Rocio; Deutsches Krebsforschungszentrum, Schamberger, Andrea; Helmholtz Zentrum München, Comprehensive Pneumology Center Stathopoulos, Georgios; Helmholtz Zentrum Munchen Deutsches Forschungszentrum fur Gesundheit und Umwelt, Comprehensive Pneumology Center (CPC) and Institute for Lung Biology and Disease

	(iLBD)
Key Words:	lung cancer, immunohistochemistry, cancer hallmarks
Abstract:	Background: Survival after curative resection of early-stage lung adenocarcinoma (LUAD) varies and prognostic biomarkers are urgently needed. Methods: Large-format tissue samples from a prospective cohort of 200 patients with resected LUAD were immunophenotyped for cancer hallmarks TP53, NF1, CD45, PD-1, PCNA, TUNEL, and FVIII, and were followed for median(95%CI) = 2.34(1.71-3.49) years. Results: Unsupervised hierarchical clustering revealed two patient subgroups with similar clinicopathologic features and genotype, but with markedly different survival: "proliferative" patients (60%) with elevated TP53, NF1, CD45, and PCNA expression had 50% 5-year overall survival while "apoptotic" patients (40%) with high TUNEL had 70% 5-year survival [HR95%CI = 2.23(1.33-3.80); P = 0.0069]. Cox regression and machine learning algorithms including random forests built clinically useful models: a score to predict overall survival and a formula and nomogram to predict tumour phenotype. The distinct LUAD phenotypes were validated in TCGA and KMplotter data and showed prognostic power supplementary to IASLC TNM stage and WHO histologic classification. Conclusions: Two molecular subtypes of LUAD exist and their identification provides important prognostic information.

Original research

Prognostic phenotypes of early-stage lung adenocarcinoma

Anne-Sophie Lamort[1,2,†], Jan Christian Kaiser[3,†], Mario A.A. Pepe[1,2], Ioannis Lilis[4], Giannoula Ntaliarda[4], Kalman Somogyi[2,5], Magda Spella[4], Sabine J. Behrend[1,2], Georgia A. Giotopoulou[1,2], Willem Kujawa[1,2], Michael Lindner[2,7], Ina Koch[2,7], Rudolf A. Hatz[2,7], Juergen Behr[2,8], Rocio Sotillo[2,5,6], Andrea C. Schamberger[1,2], and Georgios T. Stathopoulos[1,2,†,*]

[1] Comprehensive Pneumology Center (CPC) and Institute for Lung Biology and Disease (iLBD), Helmholtz Center Munich-German Research Center for Environmental Health (HMGU); Max-Lebsche-Platz 31, 81377, Munich, Bavaria, Germany
[2] German Center for Lung Research; Aulweg 130, 35392, Gießen, Hesse, Germany
[3] Institute of Radiation Medicine (IRM), Helmholtz Center Munich-German Research Center for Environmental Health (HMGU); Ingolstädter Landstraße 1, 85764, Neuherberg, Bavaria, Germany
[4] Department of Physiology, Faculty of Medicine, University of Patras; 1 Asklepiou Street, 26504, Rio, Achaia, Greece
[5] Division of Molecular Thoracic Oncology, German Cancer Research Center (DKFZ); ImNeuenheimer Feld 280, 69120, Heidelberg, Germany
[6] Translational Lung Research Center Heidelberg (TRLC), German Center for Lung Research (DZL), Heidelberg, Germany
[7] Center for Thoracic Surgery Munich, Ludwig-Maximilian-University of Munich and Asklepios Medical Center; Robert-Koch-Allee 2, 82131 Gauting, Bavaria, Germany
[8] Department of Medicine V, University Hospital, Ludwig-Maximilians-University of Munich; Marchioninistraße 15, 81377 Munich, Bavaria, Germany
† Equally contributing authors

* **Corresponding author:** Georgios T. Stathopoulos; Comprehensive Pneumology Center; Max-Lebsche-Platz 31, Munich, 81377; Germany; Phone: +49 (89) 3187 4846; Fax: +49 (89) 3187 4661; e-mail: stathopoulos@helmholtz-muenchen.de

Running Title: Molecular phenotypes of LUAD.
Keywords: lung cancer; immunohistochemistry; cancer hallmarks.
Financial Support: This work was supported by European Research Council 2010 Starting Independent Investigator (#260524) and 2015 Proof of Concept (#679345) grants, the Graduate College (Graduiertenkolleg, GRK) #2338 of the German Research Society (Deutsche Forschungsgemeinschaft, DFG), the target validation project for pharmaceutical development ALTERNATIVE of the German Ministry for Education and Research (Bundesministerium für Bildung und Forschung, BMBF), and a Translational Research Grant by the German Center for Lung Research (Deutsches Zentrum für Lungenforschung, DZL) (all to GTS). The study sponsors had no role in study design, data collection, analysis, and interpretation, and in writing and submitting the paper for publication.
Conflict of interest: The authors declare no potential conflicts of interest
Prior publication: This manuscript has not been published, accepted for publication or submitted elsewhere, either whole or in part, in any form.
Word count, manuscript: 3,011
Figures: 8
Supplementary figures/tables: 5/3
References: 30

ABSTRACT

Background: Survival after curative resection of early-stage lung adenocarcinoma (LUAD) varies and prognostic biomarkers are urgently needed.

Methods: Large-format tissue samples from a prospective cohort of 200 patients with resected LUAD were immunophenotyped for cancer hallmarks TP53, NF1, CD45, PD-1, PCNA, TUNEL, and FVIII, and were followed for median(95%CI) = 2.34(1.71-3.49) years.

Results: Unsupervised hierarchical clustering revealed two patient subgroups with similar clinicopathologic features and genotype, but with markedly different survival: "proliferative" patients (60%) with elevated TP53, NF1, CD45, and PCNA expression had 50% 5-year overall survival while "apoptotic" patients (40%) with high TUNEL had 70% 5-year survival [HR95%CI = 2.23(1.33-3.80); $P = 0.0069$]. Cox regression and machine learning algorithms including random forests built clinically useful models: a score to predict overall survival and a formula and nomogram to predict tumour phenotype. The distinct LUAD phenotypes were validated in TCGA and KMplotter data and showed prognostic power supplementary to IASLC TNM stage and WHO histologic classification.

Conclusions: Two molecular subtypes of LUAD exist and their identification provides important prognostic information.

Word count, Abstract: 170

TAKE HOME MESSAGE

Clinical-grade immunodetection of TP53, NF1, CD45, PD-1, PCNA, TUNEL, and FVIII in tumour samples identifies two phenotypes of resected lung adenocarcinomas that display different prognosis and can be used for patient management and trial design.

Character count, Take home message: 246

INTRODUCTION

Lung adenocarcinoma (LUAD), the most frequent histologic subtype of lung cancer, accounts for estimated one million annual deaths **[1,2]**. Although surgical resection remains the preferred definitive cure for early-stage LUAD **[3]**, survival thereafter is highly variable, necessitating the development and validation of prognostic biomarkers **[4]**. Such biomarkers can be clinicopathologic features **[5-7]**, genomic alterations **[8-12]**, gene expression profiles **[13,14]**, imaging characteristics **[15,16]**, and immunohistochemical expression of single markers **[17-22]**. However, no biomarker to date has found widespread applicability. Patients with resectable LUAD are currently treated with (neo)adjuvant chemo-, radio-, targeted-, and/or immuno-therapies dictated by TNM stage and driver mutations and are followed in a uniform fashion **[3,9-12]**. This is in contrast to other cancer types, where immunodetection of key tumour hallmarks dictates therapy and prognosis. For example, IHC expression of marker of proliferation Ki67 and oestrogen, progesterone, and epidermal growth factor type 2 receptors dictate treatment and prognosis in breast cancer **[23]**.

Here we analyse 200 patients with resected LUAD **[7]** using conventional (non-tissue microarray-based) immunohistochemistry (IHC) of large, representative tumour tissue areas and a clinical-grade scoring system for cancer hallmarks **[24]** tumour protein 53 (TP53), neurofibromatosis 1 (NF1), cluster of differentiation 45 (CD45), programmed cell death-1 (PD-1), proliferating cell nuclear antigen (PCNA), terminal deoxynucleotidyl nick-end labelling (TUNEL), and anti-hemophilic factor (FVIII). We follow patients for prolonged periods of time [cumulative/median(95%CI) follow-up = 507/2.34(1.71-3.49) years] to discover two phenotypes of LUAD with markedly different overall survival (OS). These phenotypes are validated in two independent datasets. Clinicians are provided with tools to predict LUAD phenotype and with proposals for their potential clinical implementation.

MATERIALS AND METHODS

Study design: The present study was conducted in accordance with the Helsinki Declaration, was prospectively approved by the Ludwig-Maximilian-University Munich Ethics Committee (#623-15) and was registered with the German Clinical Trials Register (#DRKS00012649). All patients gave written informed consent. During 2011-2017, $n = 200$ patients with full clinical data and ample available tissues were recruited for the present study, designed to reflect the whole cohort of $n = 366$ patients **[7] (Supplementary Table E1)** and to detect medium effect sizes ($d = 0.25$) with $\alpha = 0.05$ and $\beta = 0.90$ using G*Power academic software (https://www.psychologie.hhu.de/arbeitsgruppen/allgemeine-psychologie-und-arbeitspsychologie/gpower; RRID:SCR_013726).

Patient data and tumour samples: Anonymized data and samples were comprehensively reviewed by a dedicated panel (ASL, JCK, MAAP, SJB, GAG, ACS, ML, IK, RAH, JB, and GTS), including International Association for the Study of Lung Cancer (IASLC) tumour-node-metastasis (TNM) stage (the 7th edition was used due to the timing of the study) **[25]**, World Health Organization (WHO) histologic growth pattern (the 2015 classification was used) **[2,5]**, and spread through the airspaces (STAS) **[26-28]**. Tissue samples were cut into two equal parts for IHC and for DNA/RNA extraction using guanidinium thiocyanate-phenol-chloroform extraction (TRIzol; ThermoFisher, Waltham, MA).

IHC and TUNEL: Tissues were formalin-fixed (CAS #50-00-0) and paraffin-embedded (CAS #8002-74-2), cut into 5 µm-thick serial tissue sections, and stained with primary antibodies and their corresponding horseradish peroxidase-linked secondary antibodies (**Supplementary Table E2**). For negative controls, primary antibodies were omitted. Terminal deoxynucleotidyl nick-end labelling (TUNEL) was performed with the Click-it TUNEL kit (ThermoFisher). For negative controls, dUTP (CAS #94736-09) was omitted.

Slides were counterstained with hematoxylin (Roth, Karlsruhe, Germany; CAS #517-28-2) and coverslipped using Entellan (Merck, Darmstadt, Germany). Ten different areas of each tumour and five different fields of view of each tissue section were analysed by three trained blinded readers (ASL, WK, and GTS) at low magnification (x 20), the percentage of stained cells was semi-quantitatively scored as 0 (< 5%), 1 (5-24%), 2 (25-49%), 3 (50-74%), or 4 (> 74%) on an Eclipse E400 microscope (Nikon, Melville, NY; RRID:SCR_020320) using TCapture software (Tucsen Photonics, Fuzhou, China; RRID:SCR_020956), and the results were averaged by patient, as routinely done and described elsewhere **[17-20,23]**. Cancer-specific hallmark expression was also determined in randomly selected paired normal lung tissues (n = 50).

Digital droplet PCR (ddPCR): DNA was purified with GenElute Mammalian Genomic DNA Miniprep (Sigma-Aldrich, St. Louis, MO), and *KRAS* codon 12/13 and *EGFR* exon 19 were analysed with ddPCR *KRAS* G12/G13 and *EGFR* exon 19 del Screening Kits, respectively, using QuantaSoft Analysis Pro software (Bio-Rad, Hercules, CA). Data were normalized by accepted droplet numbers to yield absolute mutation allelic frequencies, and 25% mutant droplets was used as the cut-off to discriminate wild-type from mutant tumours.

***ALK* fusion detection:** 50 ng RNA was used for reverse transcription using Quantitect Reverse Transcription Kit (Qiagen, Hilden, Germany). The provider's protocol was followed, except that 0.25ul *ALK*-specific reverse primer (hAlk.cdna.rev1) was added to the primer mix to enrich transcripts carrying the 3' part of the *ALK* gene. RNA from human cell lines (NCI-H3122, *EML4-ALK* variant 1, RRID:CVCL_5160; NCI-H2228, *EML4-ALK* variant 3, RRID:CVCL_1543) served as positive controls. 10 µl PCR reactions were performed using HotStarTaq Master Mix (Quiagen) and 200 ng cDNA template. PCR products were run on 10% agarose gels. *EML4-ALK*-positive reactions were repeated, and the PCR products were

purified and sequenced to confirm *EML4-ALK* transcripts. Variant-specific forward (hEml4.cdna.v1.for1; hEml4.cDNA.v2.for1; hEml4.cdna.v3.for1) and universal reverse (hAlk.cdna.rev2) primer sequences were: hAlk.cdna.rev1, CTCCTTCAGGTCACTGATGG; hAlk.cdna.rev2, TTGCCAGCAAAGCAGTAGTTGG; hEml4.cdna.v1.for1, AGTTTCACCCAACAGATGCAAATACC; hEml4.cdna.v2.for1, TAGATGAACCAGGACACTGTGCAG; and hEml4.cdna.v3.for1 , AGCCCTCTTCACAACCTCTCC.

Computational analyses and statistics: Statistics and heatmap visualizations were done on R* (https://www.r-project.org/; RRID:SCR_001905) and GraphPad Prism v8.0 (GraphPad, San Diego, CA; https://www.graphpad.com/scientific-software/prism/; RRID:SCR_002798). Unsupervised hierarchical clustering was performed using Euclidean distance and clustering method "ward.D2" on the R* package pheatmap (https://cran.r-project.org/web/packages/pheatmap/index.html; SCR_016418). To investigate predictors of OS and prevalence of the proliferative phenotype, a combination of machine learning and regression techniques were applied. Kaplan-Meier, Cox regression, and random forests were selected to determine optimal cut-offs and OS at different end-points (one and three years). Random forests were grown using R* package randomforestSRC (https://cran.r-project.org/web/packages/randomForestSRC/index.html; RRID:SCR_015718). Co-variables for further regression analysis were confirmed based on mean decreased accuracy. From simulated random forests, non-parametric estimates of probabilities for OS depending on pertinent co-variables (TP53, NF1, CD45, PD-1, PCNA, TUNEL, and FVIII) were derived. Partial probability estimates were generated by focusing on a single co-variable of interest for which the influence of the remaining co-variables was averaged out by summation. Random forest results were used to obtain suggestions for pertinent co-variables, to guide the introduction of nonlinear categorical dependencies, and to produce a formula and a

nomogram for single patient phenotype prediction. OS analyses were done with Kaplan-Meier estimates and Cox regression (https://cran.r-project.org/web/packages/survival/index.html; RRID:SCR_021137). Moreover, survival objects were formed in R* based on right-censored follow-up and survival status which were used in random forest generation and Cox regression. The quality of data explanation for random forests was judged by area under the curve (AUC) in classification mode. However, random forests were mainly applied to guide the regression analysis and not for rigorous prediction assessment. Finally, the preferred regression models were chosen based on goodness-of-fit measured by the Akaike information criterion (AIC) and biological plausibility. To characterize the predictive power of a given model, the AUC for logistic regression and the integrated AUC (or concordance) for Cox regression were reported. Associations between variables were examined using Mann-Whitney tests, 2-way ANOVA with Sidak's post-tests, χ^2 tests, Fischer's exact tests, and Spearman's correlations. Two-tailed probabilities (P) < 0.05 were considered significant. Graphs and tables were generated on Prism v8.0 (GraphPad) and Excel (Microsoft, Redmond, WA).

RESULTS

We selected for the present study 200 patients with complete clinical information and ample LUAD and adjacent lung tissues that were representative of the originating cohort **[7] (Supplementary Table E1)**. All 200 large-format tumour samples as well as 50 randomly selected normal tumour-adjacent lung samples were immune-labelled for TP53, NF1, CD45, PD-1, PCNA, TUNEL, and FVIII, and ten independent tumour areas were scored for immunoreactivity on a clinically-relevant semi-quantitative 0 (none)-4 (highest) scale, using normal lung tissues as background controls. Average relative inter-observer variability was < 5% for any blinded reader comparison and the three scores for each sample/marker were averaged. Raw data are given in **Supplementary Figure E1** and **Supplementary Table E3**.

All seven cancer hallmarks were overexpressed in tumour compared with adjacent lung tissues **(Figure 1)**. Unsupervised hierarchical clustering of IHC data alone using Euclidean metrics identified two patient clusters: a majority cluster highly expressing the inter-correlated markers TP53, NF1, CD45, and PCNA comprised of 121 (60%) patients (hereafter called proliferative) and a minority highly TUNEL-labelled cluster encompassing 79 (40%) patients (hereafter called apoptotic) **(Figures 2a and 2b; Supplementary Figure E2)**. Interestingly, cancer hallmark IHC and the two patient clusters were only marginally or not at all correlated with clinicopathologic variables [including sex, smoking status, chronic obstructive pulmonary disease (COPD) stage, histologic growth pattern, STAS, pTNM7 stage, and oncogene status], likely reflecting something novel **(Figures 2b and 2c; Supplementary Figures E3 and E4)**. Importantly, proliferative compared with apoptotic patients displayed markedly decreased OS [5-year survival 50% versus 70%, respectively; hazard ratio 95% confidence interval (HR95%CI) = 2.23(1.33-3.80); log-rank $P = 0.0069$], while STAS and mutation status had no impact on OS **(Figure 2d)**. To validate the existence of these two molecular LUAD phenotypes, we analysed TCGA LUAD pan-cancer data (data

link: https://bit.ly/3blzgFp), which include reverse-phase protein assay data for TP53 and PCNA (but none of the other markers) from 340 patients **[29]**. Similar to our findings, TP53 and PCNA protein expression were tightly correlated, unsupervised hierarchical clustering identified two patient clusters with high (n = 134; 39%) and low (n = 206; 61%) TP53/PCNA expression, and patients with high PCNA/P53 expression ratio displayed significantly worse OS **(Figure 3)**. Collectively, these results suggest the existence of two LUAD phenotypes, proliferative and apoptotic, in two independent patient cohorts **(Figure 4a)**.

We next analysed the impact of individual cancer hallmarks on OS using univariate Kaplan-Meier estimates of our cohort stratified by optimal cut-offs defined by the KMplot custom module (http://kmplot.com/analysis/index.php?p=service&cancer=custom_plot), performed multivariate Cox regression, and grew random forests. High TP53 and PCNA expression emerged as significant predictors of worse OS by all three methods, while high CD45 expression was associated with worse OS on Cox and random forest analyses **(Figures 4b-e)**. Importantly, TP53, PCNA, and CD45 competed with important clinicopathologic predictors of OS identified previously in several independent cohorts, such as T and N stage and histologic growth pattern, as well as patient age, lung function, and smoking status **[4–7] (Figure 4f)**. In addition to TP53, PCNA, and CD45, there was also a trend for the remaining cancer hallmarks to impact OS **(Figure 5a, graphs)**. These findings show that IHC-assessed expression of stand-alone cancer hallmarks, especially TP53, PCNA, and CD45, possesses some weak prognostic power for incipient OS of resected LUAD.

To improve the prognostic power of individual cancer hallmarks and to provide clinicians with a tool to manage individual patients, all cancer hallmarks were incorporated in an unweighted immunophenotypic LUAD death score ($LADERS_{IMM}$), in homology to a clinical LUAD death score ($LADERS_{CLIN}$) developed previously **[7]**, according to cut-offs

determined by a single or a combination of methods **(Figure 5a, table)**. We designed $LADERS_{IMM}$ for easy clinical implementation on any individual patient, by incorporating high expression of TP53, NF1, CD45, PCNA, and FVIII as predictors of worse and of TUNEL and PD-1 as predictors of better OS. Indeed, 66 patients with high $LADERS_{IMM}$ (5-6 points) had 5-year overall survival of 43%, while 118 patients with intermediate $LADERS_{IMM}$ (3-4 points) 61%, and 16 patients with low $LADERS_{IMM}$ (0-2 points) 100%, with 2-3-fold hazard ratios for every low-to-intermediate-to-high $LADERS_{IMM}$ increment **(Figures 5b and c)**. When $LADERS_{IMM}$ and $LADERS_{CLIN}$ (a survival score that incorporates age, lung function, N stage, time from diagnosis to resection, and histologic growth pattern and that outperforms TNM7 stage in predicting survival) **[7]** were compared by correlation, linear regression, and κ statistic of agreement, they were only weakly related, hence they are positioned to synergize in predicting OS **(Figure 5d)**. To this end, 73 patients with intermediate or high values (≥ 3) for both scores had 25% 5-year OS, while the remaining 127 patients over 75%, for a greater than 5-fold hazard ratio **(Figure 5e)**. These data support the clinical applicability of $LADERS_{IMM}$ alone or in combination with TNM stage and other clinicopathologic prognosticators of OS in patients with resected LUAD. To validate $LADERS_{IMM}$, mRNA expression data for the seven cancer hallmarks TP53, NF1, CD45, PD-1, PCNA, TUNEL, and FVIII were sought in the KMplot lung cancer module (https://kmplot.com/analysis/index.php?p=service&cancer=lung). When good probes for our markers were not available, the most relevant genes were used (CLTA for CD45, SPATA2 for PD-1, MKI67 for PCNA, and apopain/CASP3 for TUNEL). Again, all markers independently performed similar to our cohort in predicting better or worse OS **(Figure 6a)**. When their average expression was examined (apopain/CASP3 and PD-1 were inverted similar to $LADERS_{IMM}$), the combination of cancer hallmarks equivalent to $LADERS_{IMM}$ predicted OS in all lung cancers and in LUAD, but not in squamous cell lung carcinoma

(Figure 6b). Hence cancer hallmarks TP53, NF1, CD45, PD-1, PCNA, TUNEL, and FVIII alone or combined into a score predict OS in two independent LUAD patient cohorts. We further compared $LADERS_{IMM}$ with IASLC TNM7 stage and WHO histologic subtype in predicting OS using Kaplan-Meier and Cox analyses. $LADERS_{IMM}$ was inferior to TNM7, but superior to WHO histology **(Figures 7a-c)**, and its prognostic power was stronger in patients with advanced TNM7 stage or solid growth pattern known to have poor OS **[2,5,25]**, indicating its complementarity to the TNM7 and WHO classifications.

As opposed to using individual cancer hallmarks to directly predict OS, we next examined whether cancer hallmark IHC can be integrally used to identify individual patient phenotype and to indirectly prognose OS. Using logistic regression and random forests, all cancer hallmarks except PD-1 predicted phenotype **(Figures 8a and b)**. In **Figure 8c** we provide a formula and its performance measures designed for clinical use to predict LUAD phenotype. The formula for Microsoft Excel is $P_{PROLIFERATIVE}$ = 1/(1+e^(-(-4.9+2.5*TP53+1.9*CD45+ 1.2*PCNA-1.1*TUNEL-0.7*FVIII+1.7*NF1))), where cancer hallmark scores range from 0 (none)-4 (highest). For this, we used cross-validation with the leave-one-out method. Cut-off $P_{PROLIFERATIVE}$ = 0.538 was determined for maximal specificity/sensitivity as the median of n = 200 $P_{OPTIMAL}$ from cross-validation. $P_{PROLIFERATIVE} > 0.538$ means classification of a patient as proliferative, whereas ≤ 0.538 as apoptotic. The formula is visualised as a nomogram **(Figure 8d)**, and is easily applicable (patient examples in **Supplementary Figure E5**). The receiver-operator curve of the formula **(Figure 8e)** achieves AUC = 96%, while the agreement of the formula and nomogram with actual patient phenotype was almost perfect [κ(95%CI) = 0.833(0.755-0.912)]. Formula/nomogram-predicted phenotype significantly affected OS, performing equal to actual phenotype **(Figure 8f)**. Hence cancer hallmarks collectively can determine patient phenotype using a formula or a nomogram, indirectly prognosticating OS.

DISCUSSION

Here we assessed the expression of seven key cancer hallmarks **[24]** of genomic instability (TP53), KRAS pathway activation (NF1), tumour-associated inflammation (CD45), immune checkpoint activity (PD-1), cellular proliferation (PCNA), tumour cell apoptosis (TUNEL), and angiogenesis (FVIII) in a cohort of patients with early-stage resected LUAD hypothesizing that this will aid prognosis. We examined large-format tumour and normal tissues and applied clinical-grade semi-quantitative scoring to multiple tumour areas and sections, as is done in routine pathology. Advanced statistics and machine learning identify two LUAD phenotypes solely detectable by cancer hallmarks and not any other clinical, pathologic, or molecular feature. Proliferative versus apoptotic LUAD phenotypes define OS to an extent comparable to IASLC TNM7 stage and WHO histologic pattern. A score, a formula, and a nomogram to identify LUAD phenotypes and to predict OS are provided.

The hallmarks of cancer **[24]** have streamlined our perceptions of tumour biology, but their clinical impact is still in exploration. Phenotyping of bodily cancers by clinical-grade IHC provides pertinent guidance for treatment and prognosis, with the best example being breast cancer **[23]**. However, patients with early-stage resectable LUAD are still treated in a uniform fashion, grouped with other non-small cell lung tumours **[2, 3]**, despite that multiple studies have found that TNM stage-based OS prediction can be enhanced by many clinical, pathologic, and molecular variables **[5–22]**. We examined the possibility that LUAD patients might benefit from the current approach to breast cancer, which is treated and prognosticated based on validated molecular variables including IHC expression of marker of proliferation Ki67 and oestrogen, progesterone, and epidermal growth factor type 2 receptors **[23]**. We designed the present study in order to bridge this gap, and investigated the value of IHC for cancer hallmarks in prediction of OS of LUAD patients. Indeed, we describe two LUAD

phenotypes with markedly divergent OS. These proliferative TP53^{hi}NF1^{hi}CD45^{hi}PCNA^{hi} and apoptotic TUNEL^{hi} phenotypes can be discriminated immediately after surgery with 96% accuracy, and can accurately predict OS. The findings can be readily tested in other cohorts using the score, formula, and nomogram provided and can potentially be incorporated in clinical trial design and/or patient management. For example, the findings can be used to prompt clinical and radiologic vigilance for proliferative cases, but also to enhance clinical trial design for novel adjuvant therapies. To this end, we postulate that proliferative and apoptotic patients may exhibit differential therapeutic responses to adjuvant chemo-, targeted-, and immuno-therapies post-resection, based on their differential expression of PCNA (a proliferation marker), NF1 (a KRAS inhibitor), and CD45 (an inflammatory marker).

Our findings also trigger mechanistic hypotheses on LUAD evolution. In addition to histologic growth pattern and genomic landscape **[5,9]**, epidemiologic data from atom bomb survivors **[30]** spark hypotheses on the existence of multiple molecular varieties of LUAD. The results presented here support such hypotheses: two phenotypes of LUAD are discovered solely based on expression of cancer hallmarks, which cannot be identified by driver mutation or any other clinicopathologic feature. These phenotypes may be related with early initiating events such as environmental cause, replicative stress, and/or cell of origin or, more likely in our view, with late tumour diversity emanating from divergent mutagenic processes. Whatever the reason for their existence, we provide the means for characterization of two molecular phenotypes of LUAD, which can be used for clinical management, trial design, as well as mechanistic studies on LUAD pathobiology. Notwithstanding the limitations of the present work, such as the use of an older TNM staging system and of a limited number of markers, future validation and clinical implementation of the proliferative and apoptotic phenotypes of LUAD described here may lead to therapeutic and research innovation.

AUTHORS' CONTRIBUTIONS

ML, IK, and RAH performed surgeries and procured data that were produced during surgeries; JB performed clinical and physiologic assessment; MAAP, MS, IL, GN, SJB, GAG, and ACS processed samples and provided important intellectual input; ASL and WK performed immunohistochemistry; MAAP performed ddPCR and analyzed data; KS and RS analyzed ALK fusions; ASL, JCK, and GTS designed and guided the study, analyzed data, and wrote the manuscript. All authors critically reviewed and edited the paper for important intellectual content and approved the final submitted version. ASL, JCK, and GTS had full access to all the data of the study, had final responsibility for the decision to submit it for publication, and are the guarantors of the study's integrity.

REFERENCES

1. Global Burden of Disease Cancer Collaboration, Fitzmaurice C, Abate D, et al. Global, Regional, and National Cancer Incidence, Mortality, Years of Life Lost, Years Lived With Disability, and Disability-Adjusted Life-Years for 29 Cancer Groups, 1990 to 2017: A Systematic Analysis for the Global Burden of Disease Study. JAMA Oncol 2019; 5: 1749–1768.

2. Travis WD, Brambilla E, Nicholson AG, et al. The 2015 World Health Organization Classification of Lung Tumors: Impact of Genetic, Clinical and Radiologic Advances Since the 2004 Classification. J ThoracOncol 2015; 10: 1243–1260.

3. Postmus PE, Kerr KM, Oudkerk M, et al. Early and locally advanced non-small-cell lung cancer (NSCLC): ESMO Clinical Practice Guidelines for diagnosis, treatment and follow-up. Ann Oncol 2017; 28: iv1–iv21.

4. Liang W, Zhang L, Jiang G, et al. Development and validation of a nomogram for predicting survival in patients with resected non-small-cell lung cancer. J ClinOncol 2015; 33: 861–869.

5. Ujiie H, Kadota K, Chaft JE, et al. Solid Predominant Histologic Subtype in Resected Stage I Lung Adenocarcinoma Is an Independent Predictor of Early, Extrathoracic, Multisite Recurrence and of Poor Postrecurrence Survival. J ClinOncol 2015; 33: 2877–2884.

6. Duhig EE, Dettrick A, Godbolt DB, et al. Mitosis trumps T stage and proposed international association for the study of lung cancer/american thoracic

society/europeanrespiratory society classification for prognostic value in resected stage 1 lung adenocarcinoma. J ThoracOncol 2015; 10: 673–681.

7. Klotz LV, Courty Y, Lindner M, et al. Comprehensive clinical profiling of the Gauting locoregional lung adenocarcinoma donors. Cancer Med 2019; 8: 1486–1499.

8. Warth A, Penzel R, Lindenmaier H, et al. EGFR, KRAS, BRAF and ALK gene alterations in lung adenocarcinomas: patient outcome, interplay with morphology and immunophenotype. EurRespir J 2014; 43: 872–883.

9. Qian J, Zhao S, Zou Y, et al. Genomic Underpinnings of Tumor Behavior in In Situ and Early Lung Adenocarcinoma. Am J RespirCrit Care Med 2019; 201: 697–706.

10. Izar B, Zhou H, Heist RS, et al. The prognostic impact of KRAS, its codon and amino acid specific mutations, on survival in resected stage I lung adenocarcinoma. J ThoracOncol 2014; 9: 1363–1369.

11. Blackhall FH, Peters S, Bubendorf L, et al. Prevalence and clinical outcomes for patients with ALK-positive resected stage I to III adenocarcinoma: results from the European Thoracic Oncology Platform Lungscape Project. J ClinOncol 2014; 32: 2780–2787.

12. Rizvi NA, Hellmann MD, Snyder A, et al. Cancer immunology. Mutational landscape determines sensitivity to PD-1 blockade in non-small cell lung cancer. Science 2015; 348: 124–128.

13. Cui Y, Fang W, Li C, et al. Development and Validation of a Novel Signature to Predict Overall Survival in “Driver Gene–negative” Lung Adenocarcinoma (LUAD): Results of a Multicenter Study. Clin Cancer Res 2019; 25: 1546–1556.

14. Gentles AJ, Bratman SV, Lee LJ, et al. Integrating Tumor and Stromal Gene Expression Signatures With Clinical Indices for Survival Stratification of Early-Stage Non-Small Cell Lung Cancer. J Natl Cancer Inst 2015; 107.

15. Varghese C, Rajagopalan S, Karwoski RA, et al. Computed Tomography-Based Score Indicative of Lung Cancer Aggression (SILA) Predicts the Degree of Histologic Tissue Invasion and Patient Survival in Lung Adenocarcinoma Spectrum. J ThoracOncol 2019; 14: 1419–1429.

16. Lee HY, Lee SW, Lee KS, et al. Role of CT and PET Imaging in Predicting Tumor Recurrence and Survival in Patients with Lung Adenocarcinoma: A Comparison with the International Association for the Study of Lung Cancer/American Thoracic Society/European Respiratory Society Classification of Lung Adenocarcinoma. J ThoracOncol 2015; 10: 1785–1794.

17. Takada K, Okamoto T, Shoji F, et al. Clinical Significance of PD-L1 Protein Expression in Surgically Resected Primary Lung Adenocarcinoma. J ThoracOncol 2016; 11: 1879–1890.

18. Yanagawa N, Leduc C, Kohler D, et al. Loss of phosphatase and tensin homolog protein expression is an independent poor prognostic marker in lung adenocarcinoma. J ThoracOncol 2012; 7: 1513–1521.

19. Cappuzzo F, Tallini G, Finocchiaro G, et al. Insulin-like growth factor receptor 1 (IGF1R) expression and survival in surgically resected non-small-cell lung cancer (NSCLC) patients. Ann Oncol 2010; 21: 562–567.

20. Kilvaer TK, Paulsen E-E, Khanehkenari MR, et al. The presence of intraepithelial CD45RO+ cells in resected lymph nodes with metastases from NSCLC patients is an independent predictor of disease-specific survival. Br J Cancer 2016; 114: 1145–1151.

21. Ishida T, Kaneko S, Akazawa K, et al. Proliferating cell nuclear antigen expression and argyrophilic nucleolar organizer regions as factors influencing prognosis of surgically treated lung cancer patients. Cancer Res 1993; 53: 5000–5003.

22. Duarte IG, Bufkin BL, Pennington MF, et al. Angiogenesis as a predictor of survival after surgical resection for stage I non-small-cell lung cancer. J ThoracCardiovascSurg 1998; 115: 652–658.

23. Cardoso F, Kyriakides S, Ohno S, et al. Early breast cancer: ESMO Clinical Practice Guidelines for diagnosis, treatment and follow-up. Ann Oncol 2019; 30: 1194–1220.

24. Hanahan D, Weinberg RA. Hallmarks of cancer: the next generation. Cell 2011; 144: 646–674.

25. Groome PA, Bolejack V, Crowley JJ, et al. The IASLC Lung Cancer Staging Project: validation of the proposals for revision of the T, N, and M descriptors and consequent stage groupings in the forthcoming (seventh) edition of the TNM classification of malignant tumours. J Thorac Oncol 2007; 2: 694–705.

26. Kadota K, Nitadori JI, Sima CS, et al. Tumor Spread through Air Spaces is an Important Pattern of Invasion and Impacts the Frequency and Location of Recurrences after Limited Resection for Small Stage I Lung Adenocarcinomas. J Thorac Oncol 2015; 10: 806–814.

27. Lu S, Tan KS, Kadota K, et al. Spread through Air Spaces (STAS) Is an Independent Predictor of Recurrence and Lung Cancer-Specific Death in Squamous Cell Carcinoma. J Thorac Oncol 2017; 12: 223–234.

28. Yagi Y, Aly RG, Tabata K, et al. Three-Dimensional Histologic, Immunohistochemical, and Multiplex Immunofluorescence Analyses of Dynamic Vessel Co-Option of Spread Through Air Spaces in Lung Adenocarcinoma. J ThoracOncol 2020; 15: 589–600.

29. Campbell JD, Alexandrov A, Kim J, et al. Distinct patterns of somatic genome alterations in lung adenocarcinomas and squamous cell carcinomas. Nat Genet 2016; 48:607–16.

30. Castelletti N, Kaiser JC, Simonetto C, et al. Risk of lung adenocarcinoma from smoking and radiation arises in distinct molecular pathways. Carcinogenesis 2019; 40: 1240–1250.

FIGURE LEGENDS

Figure 1. Immunophenotyping of early-stage LUAD (*n* = 200) and randomly selected adjacent normal lung tissues (*n* = 50) for seven cancer hallmarks. Data are shown as raw data points (circles) on a semi-quantitative score of 0 (no expression) to 4 (highest expression), rotated kernel density distributions (violins), medians (dashed lines), quartiles (dotted lines), patient numbers (*n*), probabilities (*P*), Mann-Whitney test, and squared Spearman's correlation coefficients for $n = 50$ tumour-normal tissue pairs (ρ^2). Note that all seven cancer hallmarks are overexpressed in cancerous compared with adjacent tissues and that expression values between the two compartments are not correlated. TP53, tumour protein 53; CD45, cluster of differentiation 45; PCNA, proliferating cell nuclear antigen; TUNEL, terminal deoxynucleotidyltransferase dUTP nick-end labelling; FVIII, coagulation factor VIII; NF1, neurofibromatosis 1; PD-1, Programmed cell death protein 1.

Figure 2. Two patient clusters of early-stage LUAD with markedly different survival. a) Heatmap shows unsupervised hierarchical clustering of $n = 200$ patients by IHC of tumour tissues for seven cancer hallmarks. Each column represents one patient and each row one marker. **b)** Heatmaps show Spearman's correlation coefficients (ρ) between immunoreactivity for the seven markers (left), as well as median parametric clinical variables (middle) and median marker expression (right) for proliferative and apoptotic patient clusters. Data are shown as ρ (left) and median values (middle and right), patient numbers (*n*), and probability (*P*), 2-way ANOVA. Left: * and **, $P < 0.05$ and $P < 0.01$, respectively, Spearman's correlation. Middle and right: ns, **, ***, and ****, $P > 0.05$, $P < 0.01$, $P < 0.001$, and $P < 0.0001$, respectively, for comparison between the two clusters, Sidak's post-test. **c)** Crosstabulations of proliferative and apoptotic cluster patient numbers (*n*) and percentages (%) stratified by non-parametric variables. *P*, probabilities, χ^2 or Fischer's exact

tests. **d)** Overall survival (OS) of all patients stratified by immunophenotypic cluster (left), spread through the airspaces (middle), and oncogene status (right). Data are shown as patient numbers (*n*), Kaplan-Meier survival estimates (lines), censored observations (line marks), survival tables, hazard ratio(95% confidence interval) (HR95%CI), and log-rank *P* values.

Figure 3. TCGA protein data support the existence of two LUAD phenotypes. TP53 and PCNA protein expression (no other from the selected markers is available) in *n* = 340 patients with LUAD from the TCGA pan-cancer dataset define two patient clusters, are tightly correlated, and determine OS. Data were retrieved from https://www.cbioportal.org/ on 03.19.2021. **a)** Heatmap shows unsupervised hierarchical clustering of *n* = 340 patients by protein expression of tumour tissues for TP53 and PCNA assessed by reverse-phase protein assay. Each row represents one patient and each column one marker. ****, probability (*P*) < 0.0001 for comparison between the two clusters, Sidak's post-test. **b)** Correlation and linear regression between TP53 and PCNA protein expression. Shown are raw data points (circles) color-coded by mutation status, Spearman's correlation coefficients and *P* values, as well as linear regression line, formula, and *P* value. **c)** OS of all patients stratified by PCNA/TP53 expression ratio. Data are shown as patient numbers (*n*), Kaplan-Meier survival estimates (lines), censored observations (line marks), survival table, hazard ratio (HR), and log-rank *P* value. Raw data were analysed using the Kaplan-Meier plotter custom module on 03.19.2021 (https://kmplot.com/analysis/index.php?p=service&cancer=custom_plot).

Figure 4. Single marker analyses targeted at overall survival. **a)** Schematic of the two identified LUAD phenotypes and their respective cancer hallmark expression patterns. **b-f)** OS analyses by single marker cut-offs optimized using univariate Kaplan-Meier estimates (b), multivariate Cox regression (c), random forest analyses with end-points set at one year

(d) and three years (e), and variable importance (VIMP) plot of variable importance rank from random forest probability (*P*) values versus minimal depth rank order from logistic regression (f). Data in b) and c) are shown as immunoreactivity cut-offs (y-axis numbers), hazard ratios (circles), and 95% confidence intervals (bars). * and **, $P < 0.05$ and $P < 0.01$, respectively, compared with hazard ratio = 1, log-rank test (b) and Cox regression (c). Data in d) and e) are shown as probability of OS by marker expression. Data in f) are shown as estimates (circles), cut-offs (dashed lines), and regression (solid line).

Figure 5. An immunophenotypic score determines survival in LUAD. a) Univariate (KM), multivariate (Cox), and random forest (RF) survival analyses identified optimized cut-offs of single marker immunoreactivity. Shown is OS of all patients stratified by single marker immunoreactivity (graphs) and composite immunophenotypic survival score (table). **b)** Patient distribution by immunophenotypic LUAD death score ($LADERS_{IMM}$). **c)** OS of all patients stratified by $LADERS_{IMM}$. **d)** Comparison of $LADERS_{IMM}$ with a previously derived clinical LUAD death score ($LADERS_{CLIN}$) shows that these are only marginally related. Shown are Spearman's correlation coefficient (ρ) and *P*, linear regression *P* and slope, as well as weighted agreement coefficient (κ). **e)** OS of all patients stratified by both $LADERS_{IMM}$ and $LADERS_{CLIN}$ [7]. Data in a), c), and e) are shown as patient numbers (*n*), Kaplan-Meier survival estimates (lines), censored observations (line marks), and probability (*P*), log-rank test, with or without hazard ratio (HR), 95% confidence interval (95%CI).

Figure 6. A gene expression profile related to immunophenotype determines survival in LUAD. Univariate OS analyses by optimized cut-offs of LUAD patients by single markers **a)** and of all lung cancer patients by median expression of all markers (apopain and SPATA2 inverted) **b)**. Data are shown as patient numbers, Kaplan-Meier survival estimates (lines),

censored observations (line marks), survival tables, hazard ratios (HR), and log-rank *P* values. Data were from the Kaplan-Meier plotter lung cancer genechip module (https://kmplot.com/analysis/index.php?p=service&cancer=lung). LUSQ, squamous cell lung carcinoma; LUAD, lung adenocarcinoma.

Figure 7. LUAD immunophenotypic score complements IASLC TNM7 stage and WHO histologic subtype. a, b) OS of all patients stratified by TNM7 stage, histologic subtype, and immunophenotypic score without (a) and with (b) category grouping shows that immunophenotypic score outperforms WHO histologic subtype and is outperformed by IASLC TNM7 stage. **c)** Results of Cox regression using TNM7 stage, histologic growth pattern, and the immunophenotypic score ($LADERS_{IMM}$) as inputs and OS as the target. AIC, Akaike's information criterion; CI ± SEM, concordance index with standard error of the mean; *P*, overall log-rank probability. **d)** OS of early- and advanced-stage patients with solid or other histologic growth patterns stratified by immunophenotype shows the increased value of the latter in advanced and solid disease. Data in a), b), and d) are shown as patient numbers (*n*), Kaplan-Meier survival estimates (lines), censored observations (line marks), and log-rank *P* values.

Figure 8. Cancer hallmarks predict LUAD phenotype and overall survival. a, b) Phenotype-predictive power of single cancer hallmarks using binary logistic regression (a) and random forest analyses (b). Data in a) are shown as hazard ratios (circles) and 95% confidence intervals (bars), with area under curve (AUC) and 95% confidence interval (95%CI). **c)** Formula with its performance measures, and **d)** nomogram for single patient phenotype prediction by integral cancer hallmark expression. Examples of how to use the formula and the nomogram are given in the text and Supplementary Figure E5. **e)** Receiver-

operator characteristic of formula/nomogram in LUAD phenotype prediction. **f)** OS of all patients stratified by formula-predicted phenotype. Data are shown as patient numbers (*n*), Kaplan-Meier survival estimates (lines), censored observations (line marks), hazard ratio (HR), and log-rank *P* value.

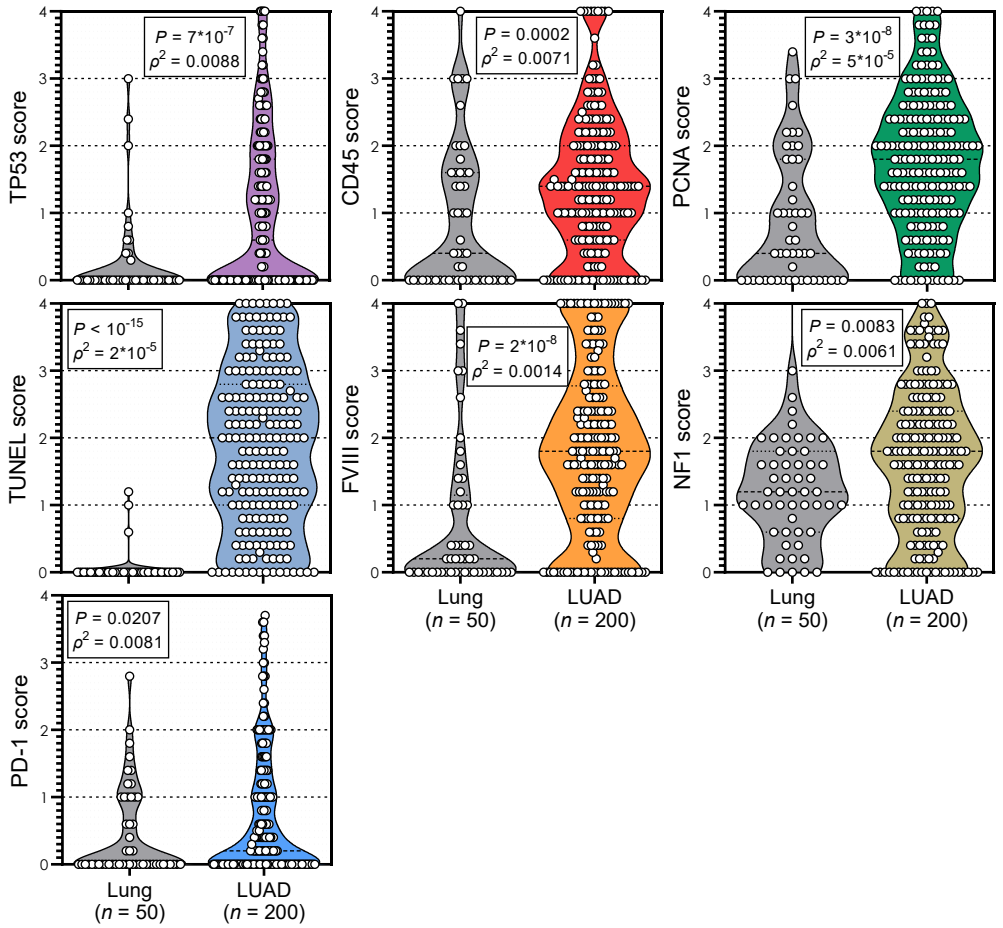

Lamort et al. Figure 1. Immunophenotyping of early-stage LUAD (*n* = 200) and randomly selected adjacent normal lung tissues (*n* = 50) for seven cancer hallmarks. Data are shown as raw data points (circles) on a semi-quantitative score of 0 (no expression) to 4 (highest expression), rotated kernel density distributions (violins), medians (dashed lines), quartiles (dotted lines), patient numbers (*n*), probabilities (*P*), Mann-Whitney test, and squared Spearman's correlation coefficients for $n = 50$ tumour-normal tissue pairs (ρ^2). Note that all seven cancer hallmarks are overexpressed in cancerous compared with adjacent tissues and that expression values between the two compartments are not correlated. TP53, tumour protein 53; CD45, cluster of differentiation 45; PCNA, proliferating cell nuclear antigen; TUNEL, terminal deoxynucleotidyltransferase dUTP nick-end labelling; FVIII, coagulation factor VIII; NF1, neurofibromatosis 1; PD-1, Programmed cell death protein 1.

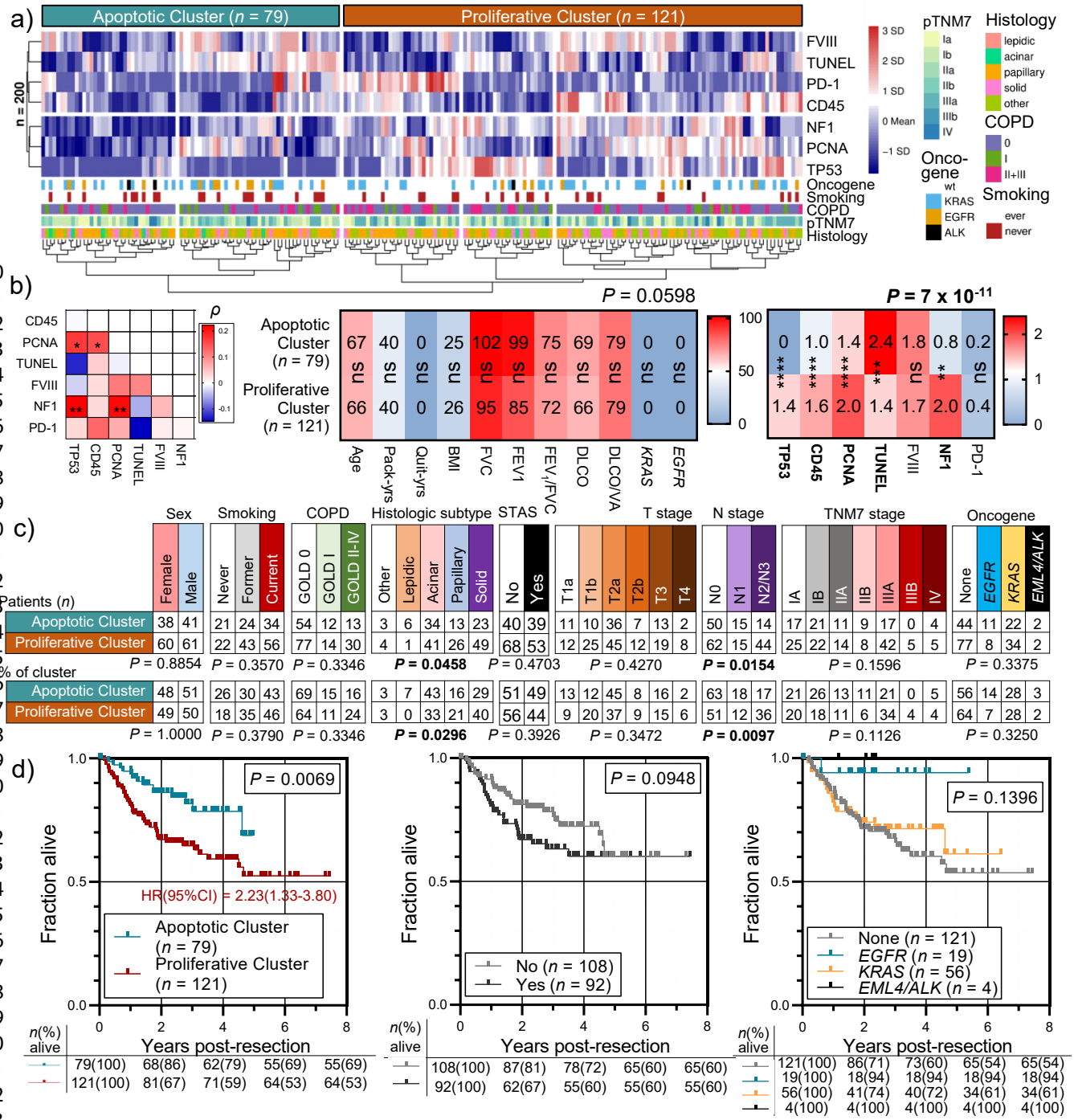

Lamort et al. Figure 2. Two patient clusters of early-stage LUAD with markedly different survival. a) Heatmap shows unsupervised hierarchical clustering of $n = 200$ patients by IHC of tumour tissues for seven cancer hallmarks. Each column represents one patient and each row one marker. **b)** Heatmaps show Spearman's correlation coefficients (ρ) between immunoreactivity for the seven markers (left), as well as median parametric clinical variables (middle) and median marker expression (right) for proliferative and apoptotic patient clusters. Data are shown as ρ (left) and median values (middle and right), patient numbers (n), and probability (P), 2-way ANOVA. Left: * and **, $P < 0.05$ and $P < 0.01$, respectively, Spearman's correlation. Middle and right: ns, **, ***, and ****, $P > 0.05$, $P < 0.01$, $P < 0.001$, and $P < 0.0001$, respectively, for comparison between the two clusters, Sidak's post-test. **c)** Crosstabulations of proliferative and apoptotic cluster patient numbers (n) and percentages (%) stratified by non-parametric variables. P, probabilities, χ^2 or Fischer's exact tests. **d)** Overall survival (OS) of all patients stratified by immunophenotypic cluster (left), spread through the airspaces (middle), and oncogene status (right). Data are shown as patient numbers (n), Kaplan-Meier survival estimates (lines), censored observations (line marks), survival tables, hazard ratio(95% confidence interval) (HR95%CI), and log-rank P values.

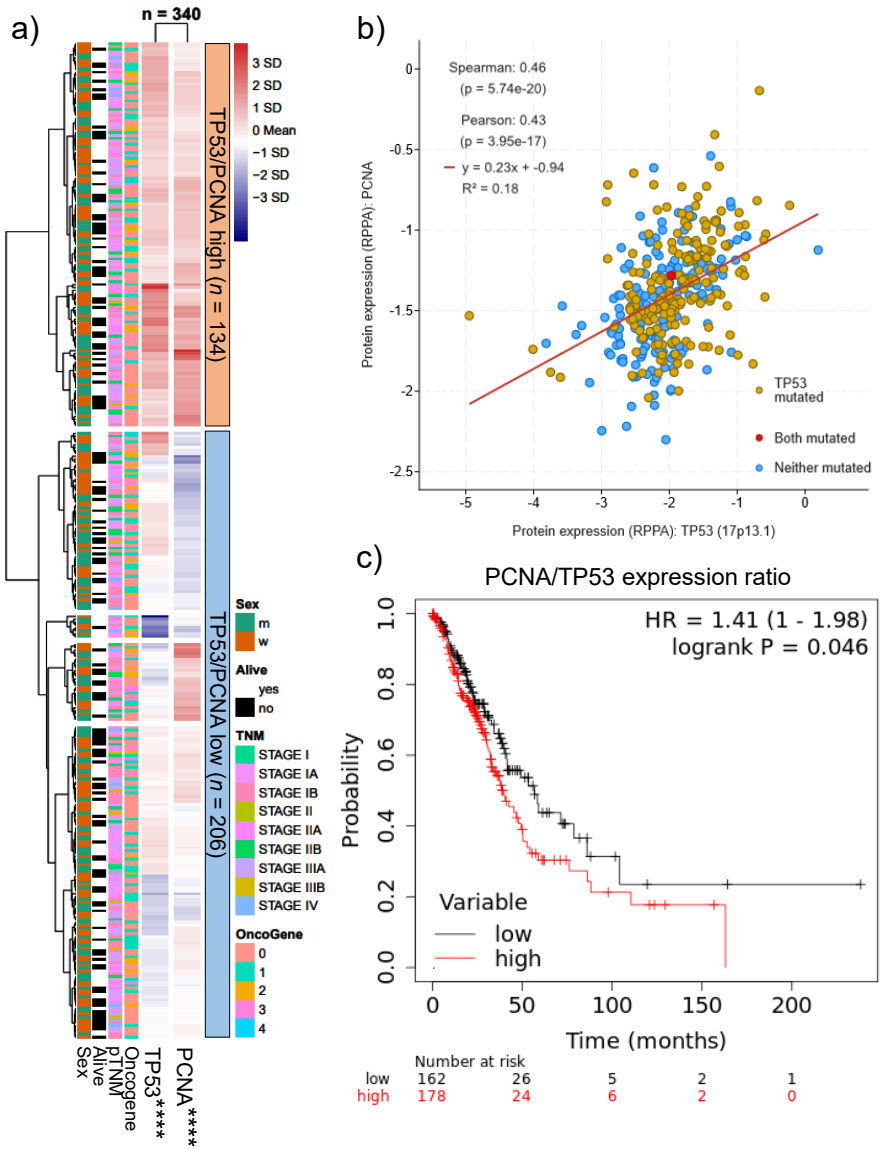

Lamort et al. Figure 3. TCGA protein data support the existence of two LUAD phenotypes. TP53 and PCNA protein expression (no other from the selected markers is available) in $n = 340$ patients with LUAD from the TCGA pan-cancer dataset define two patient clusters, are tightly correlated, and determine OS. Data were retrieved from https://www.cbioportal.org/ on 03.19.2021. **a)** Heatmap shows unsupervised hierarchical clustering of $n = 340$ patients by protein expression of tumour tissues for TP53 and PCNA assessed by reverse-phase protein assay. Each row represents one patient and each column one marker. ****, probability (P) < 0.0001 for comparison between the two clusters, Sidak's post-test. **b)** Correlation and linear regression between TP53 and PCNA protein expression. Shown are raw data points (circles) color-coded by mutation status, Spearman's correlation coefficients and P values, as well as linear regression line, formula, and P value. **c)** OS of all patients stratified by PCNA/TP53 expression ratio. Data are shown as patient numbers (n), Kaplan-Meier survival estimates (lines), censored observations (line marks), survival table, hazard ratio (HR), and log-rank P value. Raw data were analysed using the Kaplan-Meier plotter custom module on 03.19.2021 (https://kmplot.com/analysis/index.php?p=service&cancer=custom_plot).

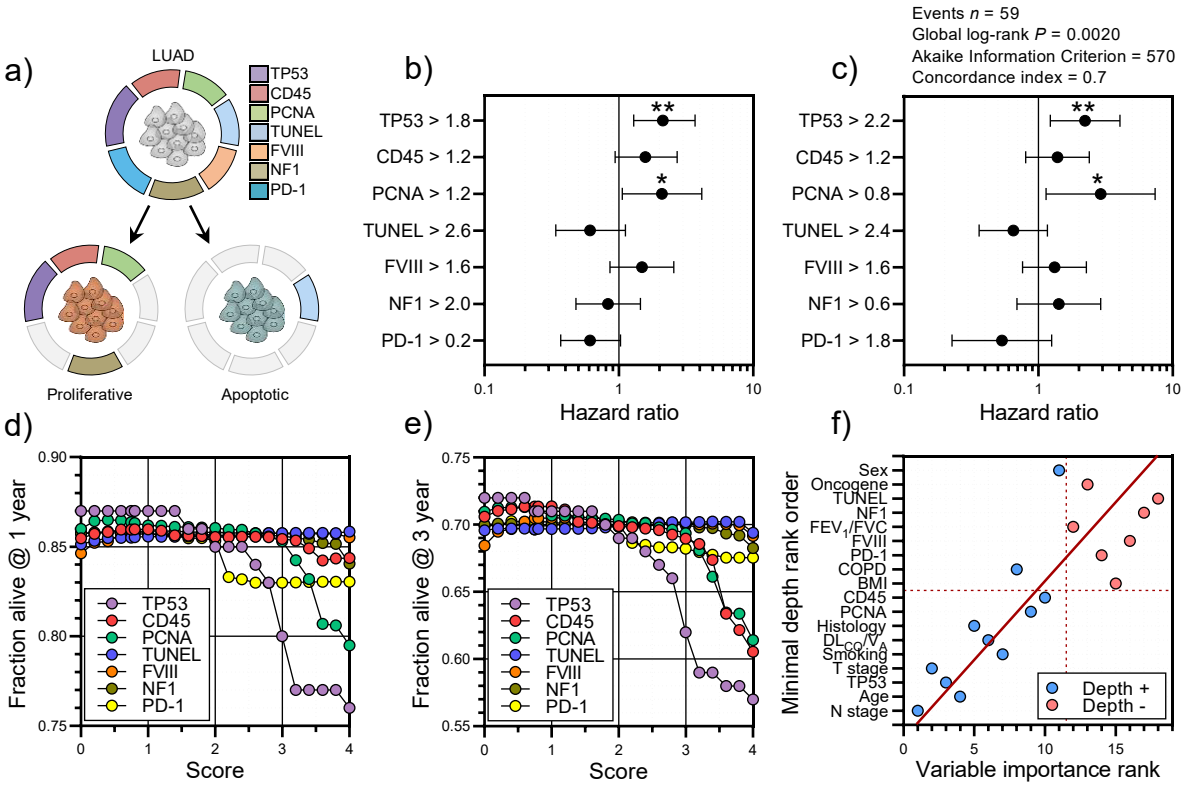

Lamort et al. Figure 4. Single marker analyses targeted at overall survival. a) Schematic of the two identified LUAD phenotypes and their respective cancer hallmark expression patterns. **b-f)** OS analyses by single marker cut-offs optimized using univariate Kaplan-Meier estimates (b), multivariate Cox regression (c), random forest analyses with end-points set at one year (d) and three years (e), and variable importance (VIMP) plot of variable importance rank from random forest probability (*P*) values versus minimal depth rank order from logistic regression (f). Data in b) and c) are shown as immunoreactivity cut-offs (y-axis numbers), hazard ratios (circles), and 95% confidence intervals (bars). * and **, $P < 0.05$ and $P < 0.01$, respectively, compared with hazard ratio = 1, log-rank test (b) and Cox regression (c). Data in d) and e) are shown as probability of OS by marker expression. Data in f) are shown as estimates (circles), cut-offs (dashed lines), and regression (solid line).

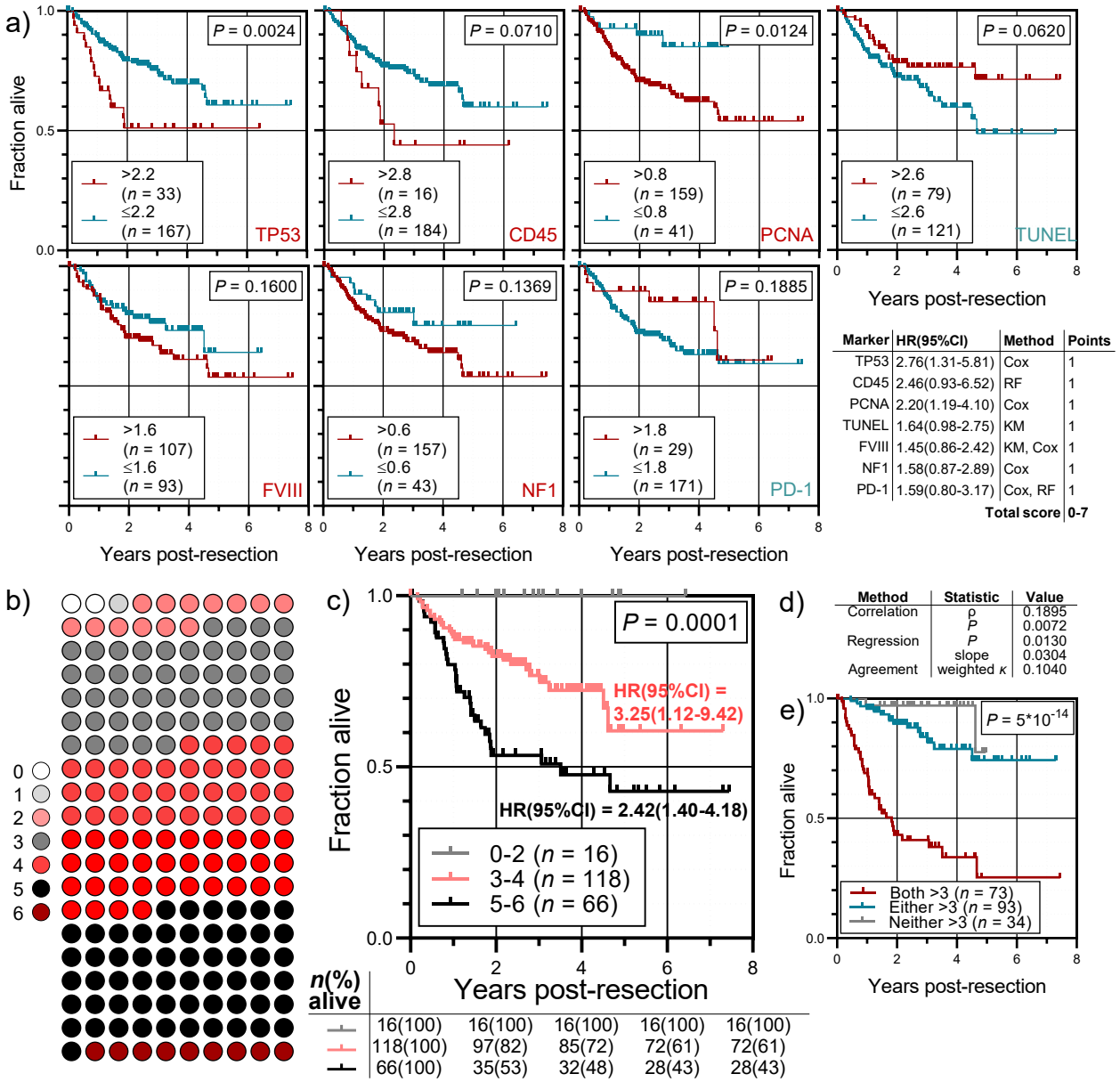

Lamort et al. Figure 5. An immunophenotypic score determines survival in LUAD. a) Univariate (KM), multivariate (Cox), and random forest (RF) survival analyses identified optimized cut-offs of single marker immunoreactivity. Shown is OS of all patients stratified by single marker immunoreactivity (graphs) and composite immunophenotypic survival score (table). **b)** Patient distribution by immunophenotypic LUAD death score ($LADERS_{IMM}$). **c)** OS of all patients stratified by $LADERS_{IMM}$. **d)** Comparison of $LADERS_{IMM}$ with a previously derived clinical LUAD death score ($LADERS_{CLIN}$) shows that these are only marginally related. Shown are Spearman's correlation coefficient (ρ) and P, linear regression P and slope, as well as weighted agreement coefficient (κ). **e)** OS of all patients stratified by both $LADERS_{IMM}$ and $LADERS_{CLIN}$ [7]. Data in a), c), and e) are shown as patient numbers (n), Kaplan-Meier survival estimates (lines), censored observations (line marks), and probability (P), log-rank test, with or without hazard ratio (HR), 95% confidence interval (95%CI).

a)

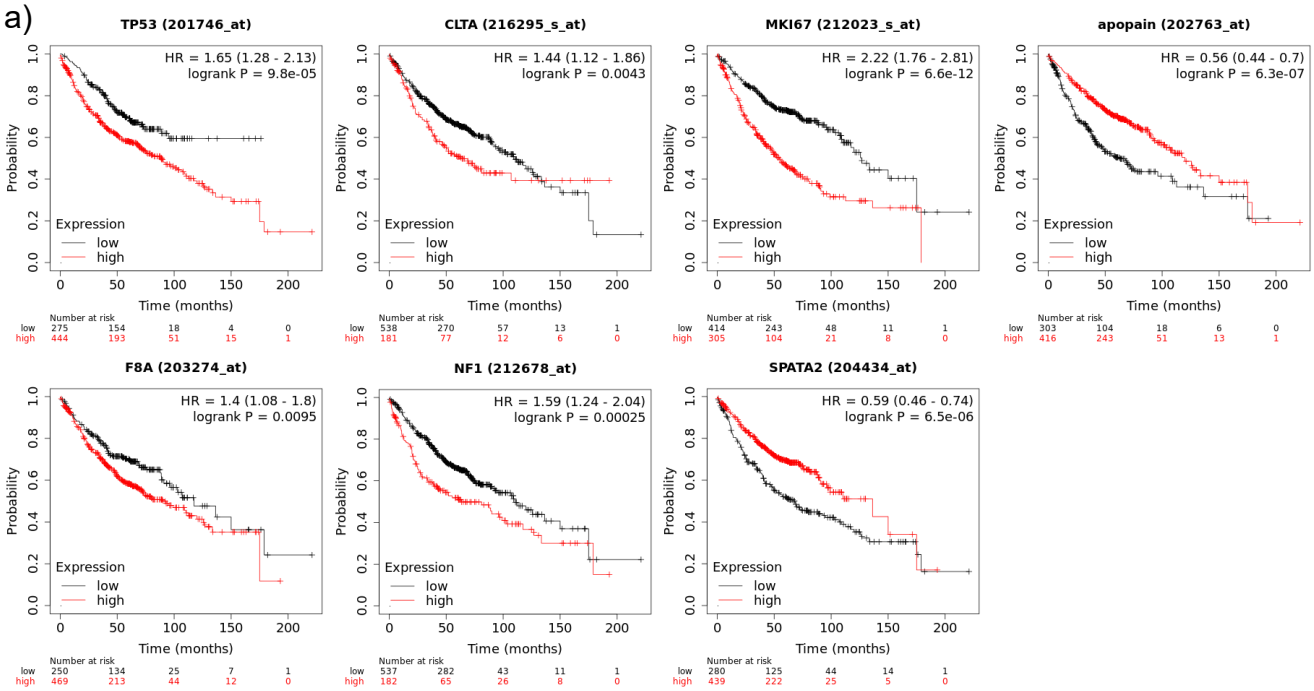

b)

Marker	KMplot RNA	KMplot probe	Weight
TP53	TP53	201746	+1
CD45	CLTA	216295	+1
PCNA	MKI67	212023	+1
TUNEL	CASP3	202763	-1
FVIII	F8A	203274	+1
NF1	NF1	212678	+1
PD-1	PD1	204434	-1

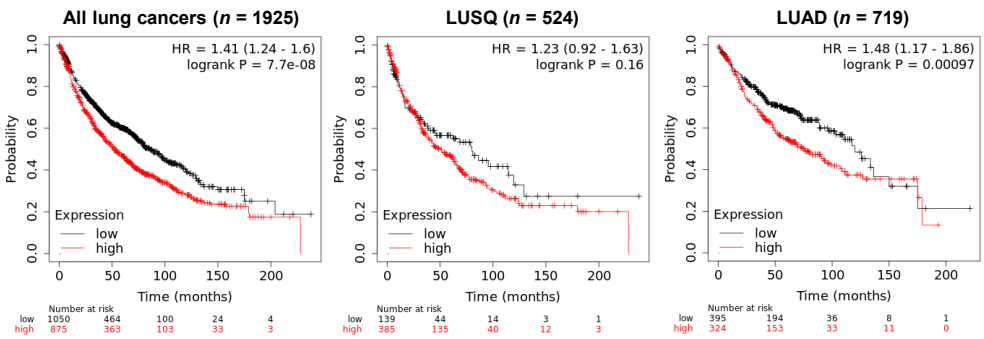

Lamort et al. Figure 6. A gene expression profile related to immunophenotype determines survival in LUAD. Univariate OS analyses by optimized cut-offs of LUAD patients by single markers **a)** and of all lung cancer patients by median expression of all markers (apopain and SPATA2 inverted) **b)**. Data are shown as patient numbers, Kaplan-Meier survival estimates (lines), censored observations (line marks), survival tables, hazard ratios (HR), and log-rank *P* values. Data were from the Kaplan-Meier plotter lung cancer genechip module (https://kmplot.com/analysis/index.php?p=service&cancer=lung). LUSQ, squamous cell lung carcinoma; LUAD, lung adenocarcinoma.

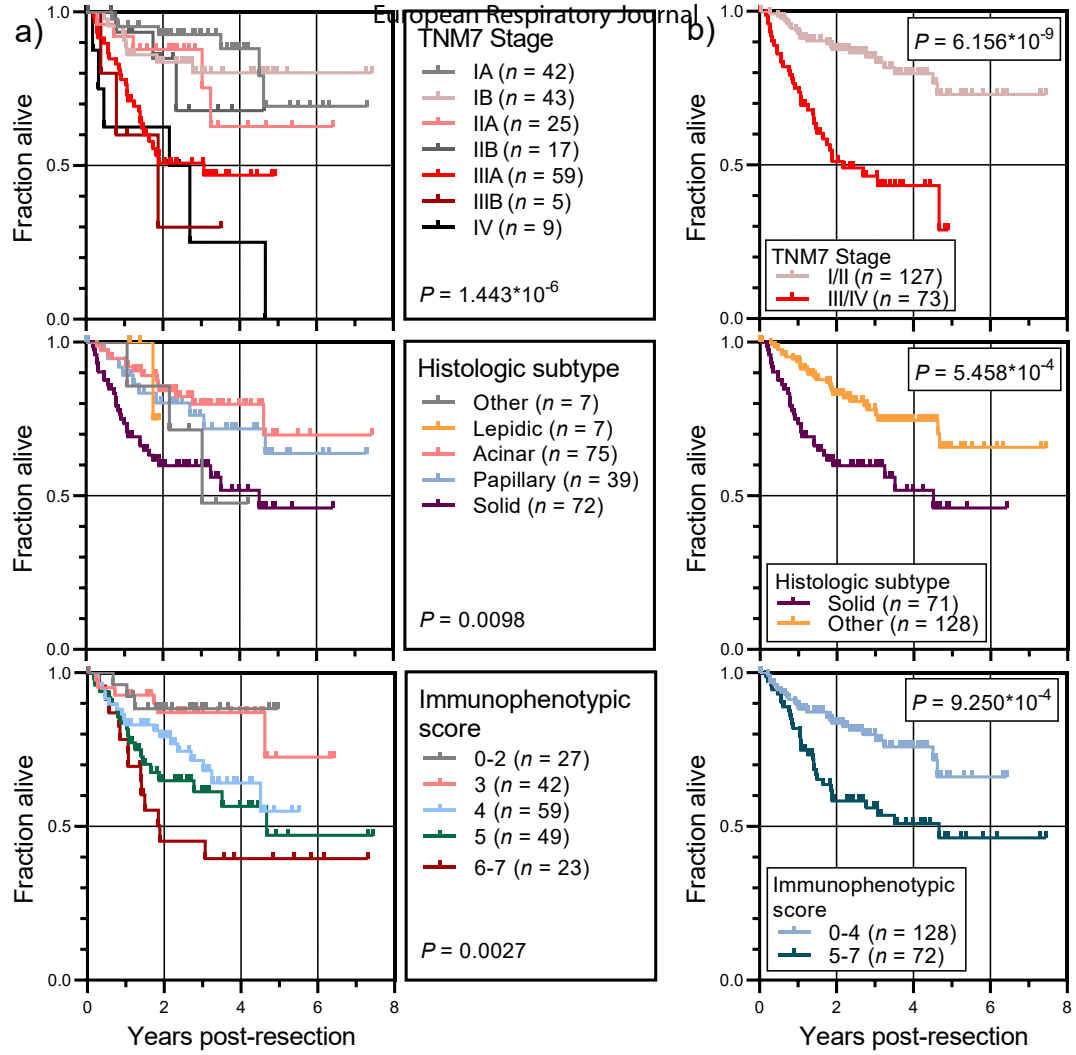

c)

Cox regression	AIC	CI ± SEM	P
TNM7	558	0.706 ± 0.033	0.004
Histology	574	0.639 ± 0.036	0.0126
LADERS$_{IMM}$	571	0.649 ± 0.036	1.462*10-5

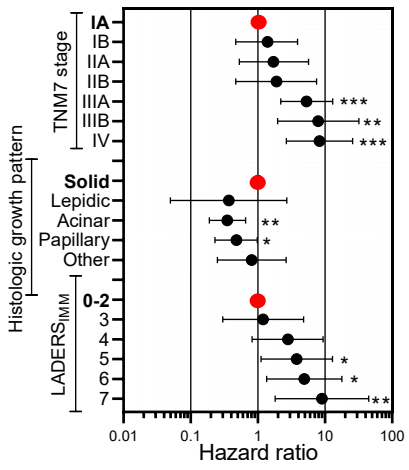

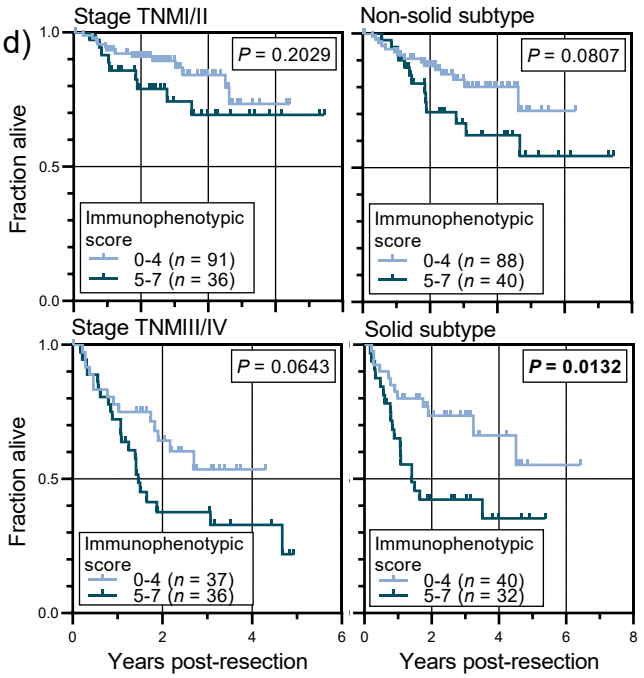

Lamort et al. Figure 7. LUAD immunophenotypic score complements IASLC TNM7 stage and WHO histologic subtype. a, b) OS of all patients stratified by TNM7 stage, histologic subtype, and immunophenotypic score without (a) and with (b) category grouping shows that immunophenotypic score outperforms WHO histologic subtype and is outperformed by IASLC TNM7 stage. **c)** Results of Cox regression using TNM7 stage, histologic growth pattern, and the immunophenotypic score (LADERS$_{IMM}$) as inputs and OS as the target. AIC, Akaike's information criterion; CI ± SEM, concordance index with standard error of the mean; *P*, overall log-rank probability. **d)** OS of early- and advanced-stage patients with solid or other histologic growth patterns stratified by immunophenotype shows the increased value of the latter in advanced and solid disease. Data in a), b), and d) are shown as patient numbers (*n*), Kaplan-Meier survival estimates (lines), censored observations (line marks), and log-rank *P* values.

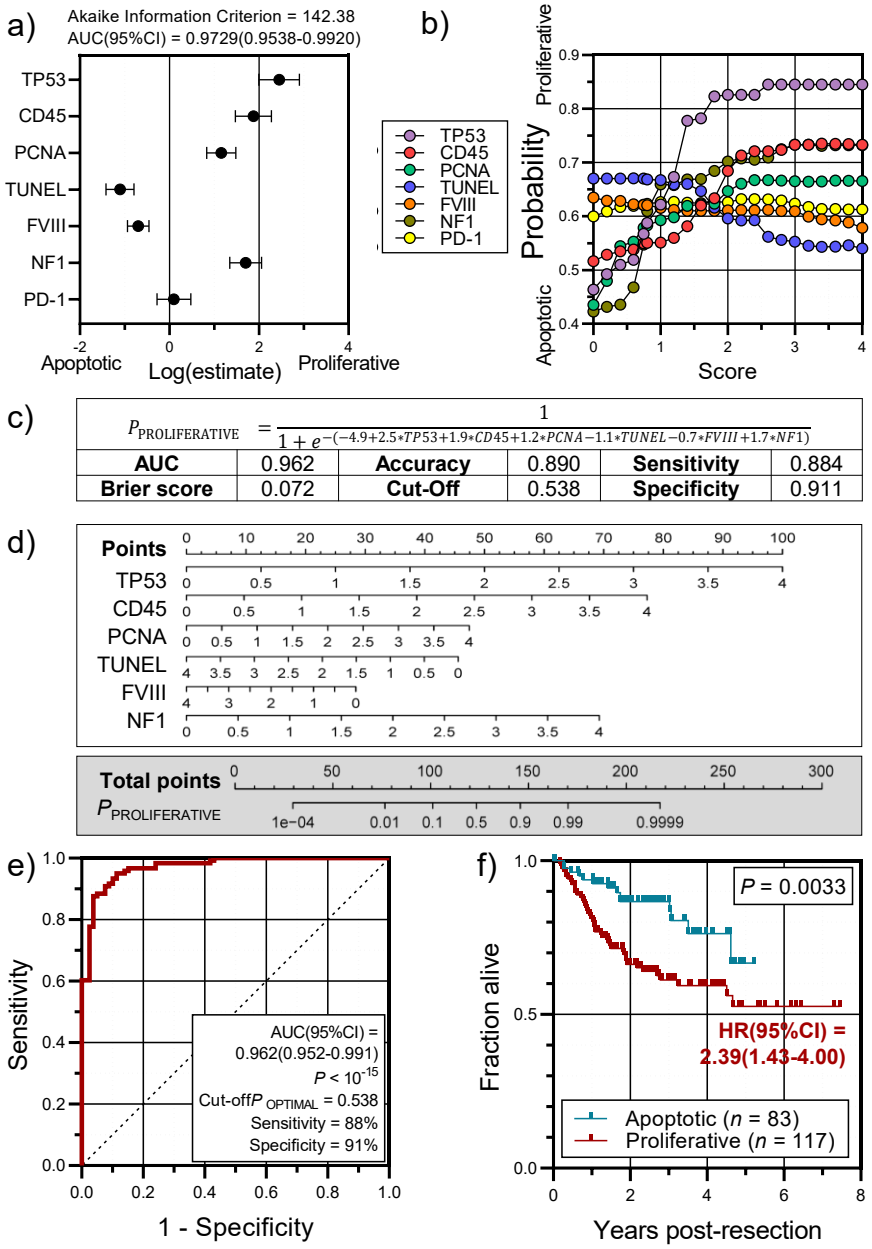

Lamort et al. Figure 8. Cancer hallmarks predict LUAD phenotype and overall survival. a, b) Phenotype-predictive power of single cancer hallmarks using binary logistic regression (a) and random forest analyses (b). Data in a) are shown as hazard ratios (circles) and 95% confidence intervals (bars), with area under curve (AUC) and 95% confidence interval (95%CI). **c)** Formula with its performance measures, and **d)** nomogram for single patient phenotype prediction by integral cancer hallmark expression. Examples of how to use the formula and the nomogram are given in the text and Supplementary Figure E5. **e)** Receiver-operator characteristic of formula/nomogram in LUAD phenotype prediction. **f)** OS of all patients stratified by formula-predicted phenotype. Data are shown as patient numbers (*n*), Kaplan-Meier survival estimates (lines), censored observations (line marks), hazard ratio (HR), and log-rank *P* value.

ONLINE SUPPLEMENTARY DATA

Prognostic phenotypes of early-stage lung adenocarcinoma

Anne-Sophie Lamort, Jan Christian Kaiser, Mario A.A. Pepe, Ioannis Lilis, Giannoula Ntaliarda, Kalman Somogyi, Magda Spella, Sabine J. Behrend, Georgia A. Giotopoulou, Willem Kujawa, Michael Lindner, Ina Koch, Rudolf A. Hatz, Juergen Behr, Rocio Sotillo, Andrea C. Schamberger, and Georgios T. Stathopoulos

TABLE OF CONTENTS

SUPPLEMENTARY TABLES

Supplementary Table E1. Comparison of the patients selected for the present study with the originating cohort.

	All patients (*n* = 366)		**Selected patients (*n* = 200)**		**Probability**
	Patients	Percentage	Patients	Percentage	χ^2 test
Smoking status					
Never	75	20	43	21	0.8850
Former	130	36	67	34	
Current	161	44	90	45	
Age					
< 45 years	11	3	7	3	0.9434
45 – 65 years	160	44	88	44	
> 65 years	195	53	105	53	
Sex					
Female	181	49	98	49	0.9301
Male	185	51	102	51	
Tumor location					
Right lung	163	45	98	49	0.1723
Left lung	133	36	76	38	
Other	70	19	26	13	
pTNM7 stage					
Ia	78	21	42	21	0.4335
Ib	60	16	43	21	
IIa	54	15	25	13	
IIb	36	10	17	9	
IIIa	97	26	59	29	
IIIb	10	3	5	3	
IV	31	9	9	4	
Histology					
Lepidic	16	4	7	4	0.9841
Acinar	14	39	75	37	
Papillary	70	19	39	19	
Solid	126	34	72	36	
Other	13	4	7	4	

SupplementaryTable E2. Antibodies used in the present study.

Target	Host	Provider	RRID	Dilution	Conjugate	Incubation
Primary						
Proliferating cell nuclear antigen, PCNA	Rabbit	Sigma-Aldrich, St. Louis, MO	AB_1855078	1:100	-	2h00 – 37°C
Tumor protein 53, TP53	Mouse	Thermo Fisher, Waltham, MA	AB_10989883	1:100	-	overnight– 4°C
Cluster of differentiation 45, CD45	Rabbit	Thermo Fisher, Waltham, MA	AB_2174009	1:250	-	overnight – 4°C
Anti-hemophillic factor VIII, FVIII	Sheep	Thermo Fisher, Waltham, MA	AB_2262541	1:500	-	2h00 – 20°C
Neurofibromin 1, NF1	Rabbit	Thermo Fisher, Waltham, MA	AB_2149657	1:500	-	overnight – 20°C
Programmed cell death-1, PD-1	Mouse	Elabscience, Houston, TX	AB_2891227	1:100	-	overnight– 4°C
Secondary						
Mouse IgG/IgM	Goat	Jackson, Cambridge, UK	AB_2338505	1:1000	horseradish peroxidase	1h30 – 20°C
Rabbit IgG	Mouse	Abcam, London, UK	AB_2650595	1:5000	horseradish peroxidase	1h30 – 20°C
Goat IgG with Sheep reactivity	Mouse	Santa Cruz Biotechnology, Dallas, TX	AB_628490	1:50	horseradish peroxidase	1h00 – 20°C

RRID, research reagent identification.
Ig, Immunoglobulin.

Supplementary Table E3. Raw data obtained from 200 resected lung adenocarcinoma donors.

Provided as a separate *.xlsx file. Clinical and molecular variables (color-coded columns) of 200 lung adenocarcinoma donors where each row represents a patient. pTNM7, pathological tumor-node-metastasis staging system seventh edition; STAS, spread through the airspaces; TP53, tumor protein 53; CD45, cluster of differentiation 45; PCNA, proliferating cell nuclear antigen; TUNEL, terminal deoxynucleotidyl transferase dUTP nick-end labeling; FVIII, coagulation factor VIII; NF1, neurofibromatosis 1; PD-1, Programmed cell death protein 1; *KRAS*, KRAS proto-oncogene, GTPase; *EGFR*, epidermal growth factor receptor; numbers 0–4, semi-quantitative immunohistochemistry scores; $LADERS_{CLIN}$, clinical LUAD death score; $LADERS_{IMM}$, immunophenotypic score.

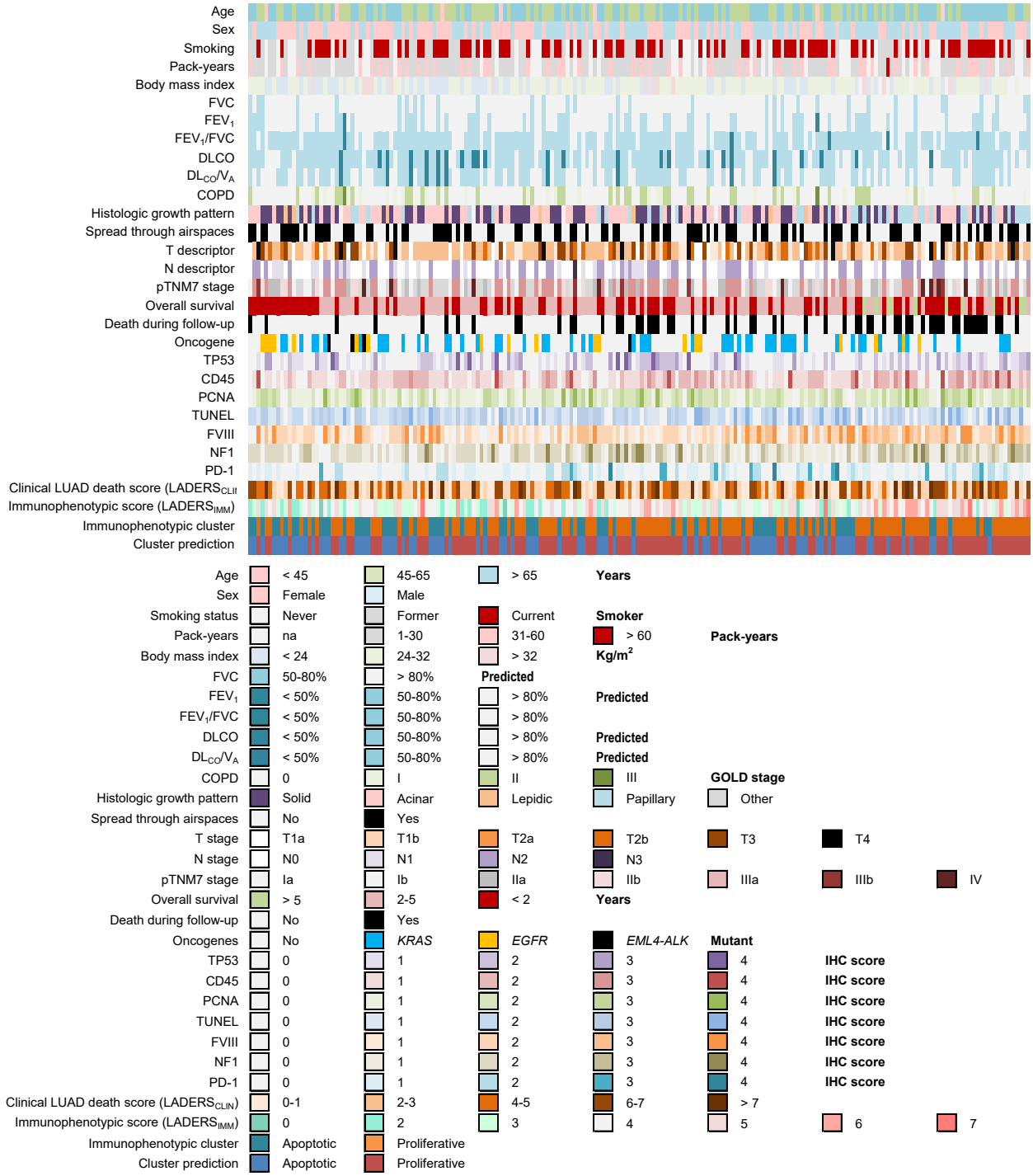

Supplementary Figure E1. Main findings of the study. Color-coded clinical and molecular variables (columns) of 200 lung adenocarcinoma donors where each column represents a patient. pTNM7, pathological tumour-node-metastasis staging system seventh edition; TP53, tumour protein 53; CD45, cluster of differentiation 45; PCNA, proliferating cell nuclear antigen; TUNEL, terminal deoxynucleotidyltransferase dUTP nick-end labelling; FVIII, coagulation factor VIII; NF1, neurofibromatosis 1; PD-1, Programmed cell death protein 1; *KRAS*, KRAS proto-oncogene, GTPase; *EGFR*, epidermal growth factor receptor; numbers 0–4, semi-quantitative immunohistochemistry scores; $LADERS_{CLIN}$, clinical LUAD death score; $LADERS_{IMM}$, immunophenotypic score.

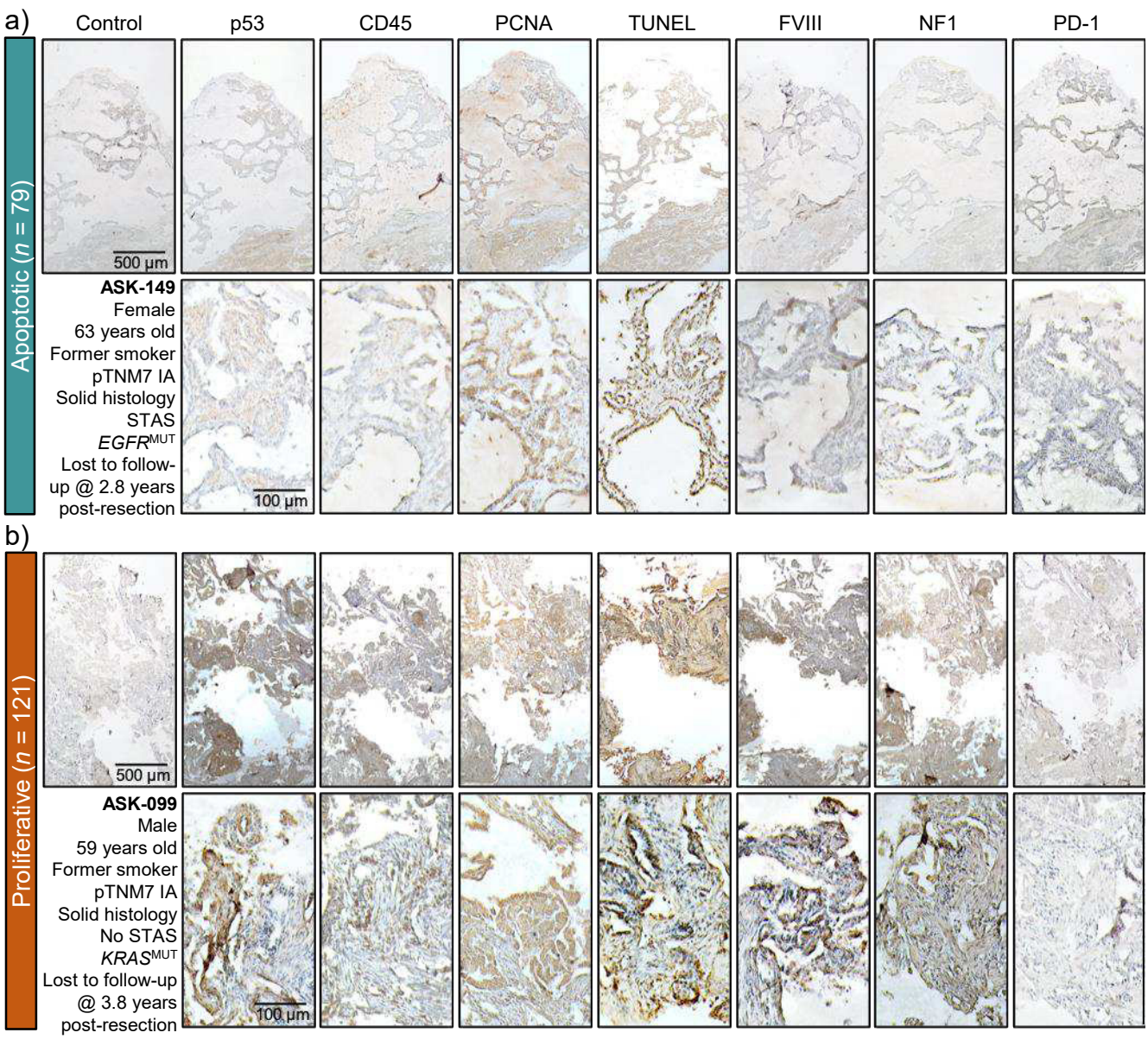

Supplementary Figure E2. Representative patients' immunoreactivity. Shown are representative immunohistochemistry microphotographs of one patient from each immunophenotype.

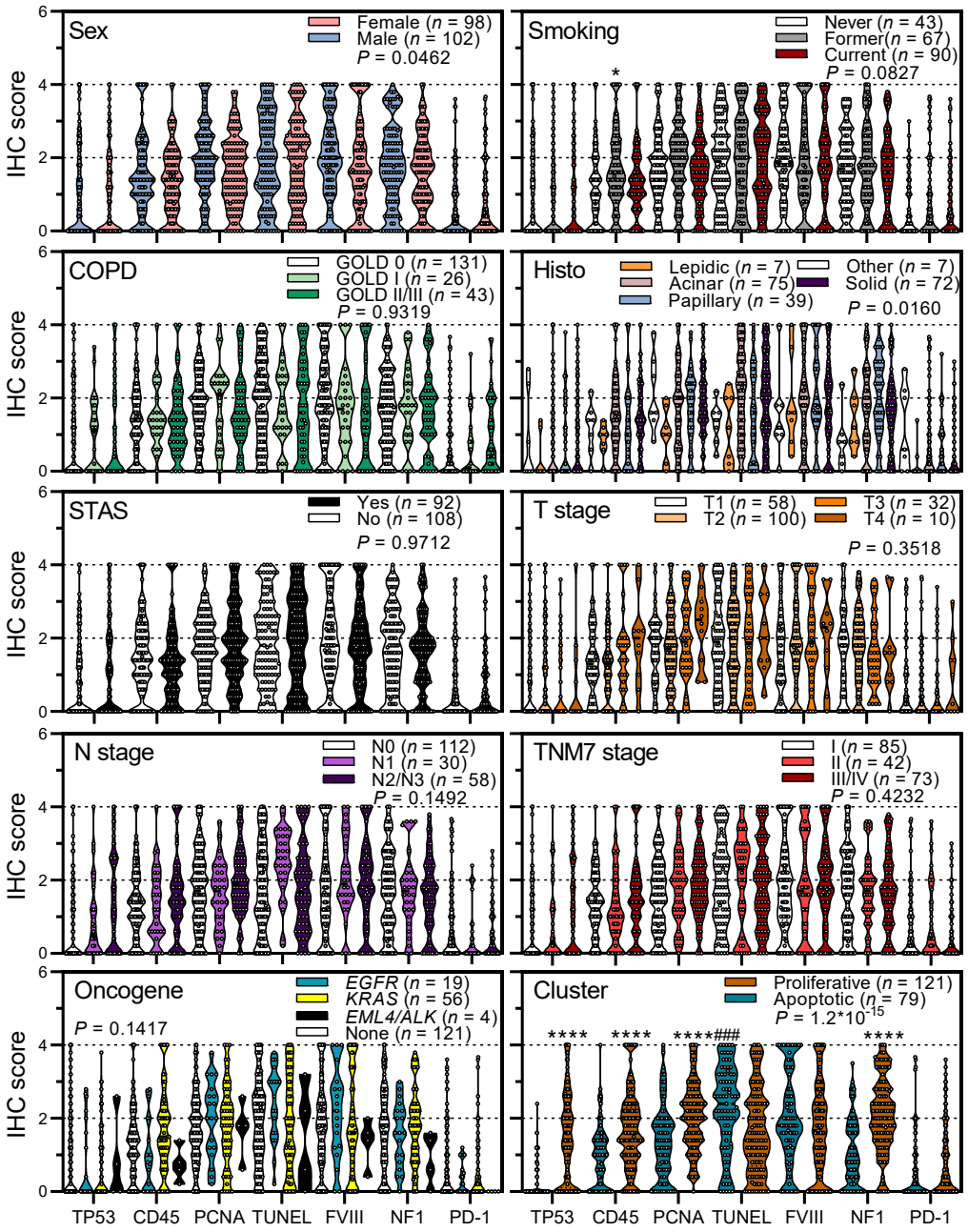

Supplementary Figure E3. Immunoreactivity of early-stage LUAD for seven cancer hallmarks. Immunoreactivity scores of tumour tissues of $n = 200$ patients with LUAD for seven cancer hallmarks stratified by clinicopathologic features shows phenotypic cluster to be the main defining factor of hallmark expression. Data are shown as patient numbers (n), raw data points (circles), rotated kernel density distributions (violins), medians (dashed lines), quartiles (dotted lines), and P, 2-way ANOVA probability values (P). *, $P < 0.05$ for comparison between former and never-smokers; ****, $P < 0.0001$ for comparison between proliferative over apoptotic patients; ###, $P < 0.001$ for comparison between apoptotic over proliferative patients; Sidak's post-test. TP53, tumour protein 53; CD45, cluster of differentiation 45; PCNA, proliferating cell nuclear antigen; TUNEL, terminal deoxynucleotidyl nick-end labelling; FVIII, anti-hemophilic factor; NF1, neurofibromatosis 1; PD-1, programmed cell death-1.

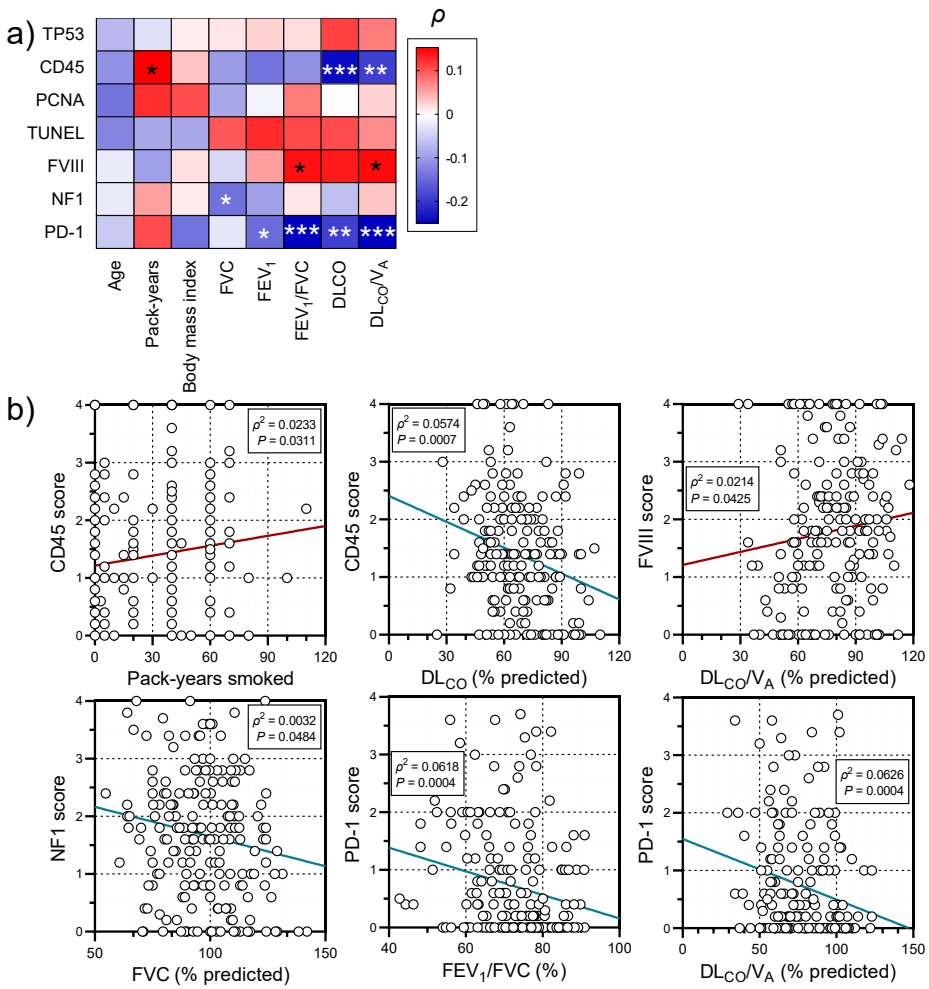

Supplementary Figure E4. Correlations between clinical variables and immunoreactivity of early-stage LUAD for seven cancer hallmarks. Immunoreactivity scores of tumor tissues of $n = 200$ patients with LUAD for seven cancer hallmarks were determined and were correlated with clinical and laboratory features. Data in **a)** are shown as heatmap of Spearman's correlation coefficients (ρ). *, **, and ***, $P < 0.05$, $P < 0.01$, and $P < 0.001$, respectively, Spearman's correlation. Data in **b)** are shown as raw data points (circles), linear regression lines (coloured lines), and squared Spearman's correlation coefficients (ρ^2) and probabilities (P) of some representative correlations. TP53, tumour protein 53; CD45, cluster of differentiation 45; PCNA, proliferating cell nuclear antigen; TUNEL, terminal deoxynucleotidyl nick-end labelling; FVIII, anti-hemophilic factor; NF1, neurofibromatosis 1; PD-1, programmed cell death-1.

a)

Patient ASK-033
Age 68 years; female never smoker; Papillary growth pattern; *EGFR* mutation; No STAS; TNM7 stage T3N2M0 (IIIA).
Lost to follow-up 3.64 years post-resection.
Immunoscores TP53 = 0.0; CD45 = 0.0; PCNA = 1.2; TUNEL = 1.6; FVIII = 2.6; NF1 = 3.0; PD-1 = 0.0
$LADERS_{CLIN}$ = 6
$LADERS_{IMM}$ = 4
Apoptotic cluster
Formula $P_{PROLIFERATIVE}$ = 0.1186
Nomogram points = 103.5
Nomogram $P_{PROLIFERATIVE}$ ~ 0.1100

b)

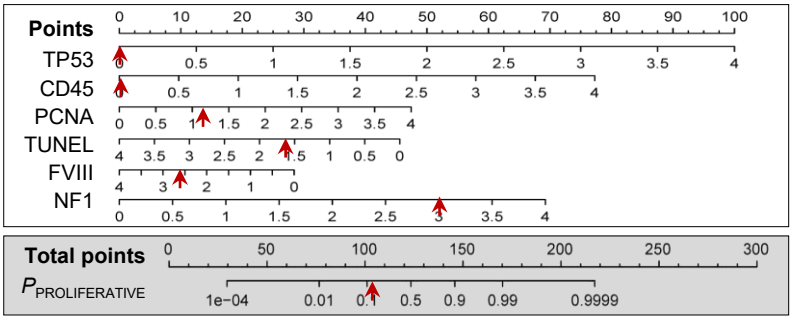

c)

Patient ASK-053
Age 74 years; male current smoker; Solid growth pattern; No known mutation; STAS; TNM7 stage T3N2M0 (IIIA).
Deceased 0.31 years post-resection.
Immunoscores TP53 = 2.0; CD45 = 1.4; PCNA = 3.0; TUNEL = 1.0; FVIII = 2.4; NF1 = 1.4; PD-1 = 0.0
$LADERS_{CLIN}$ = 10
$LADERS_{IMM}$ = 7
Proliferative cluster
Formula $P_{PROLIFERATIVE}$ = 0.9968
Nomogram points = 184.0
Nomogram $P_{PROLIFERATIVE}$ ~ 0.9960

d)

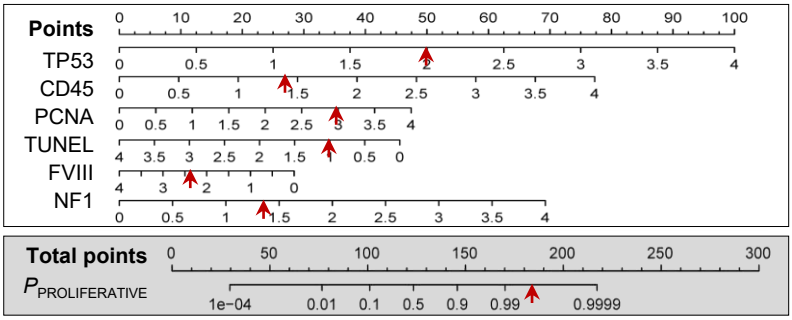

Supplementary Figure E5. Exemplary patient cluster prediction using the formula and nomogram provided. a, c) Clinical and immunoreactivity features, clinical ($LADERS_{CLIN}$) and immunoreactivity ($LADERS_{IMM}$) risk scores and probability of belonging to the proliferative phenotype ($P_{PROLIFERATIVE}$) of two representative patients, as derived from the formula and the nomogram using a cut-off of $P_{PROLIFERATIVE} > 0.538$. **b, d)** Exemplary uses of the nomogram with red arrows in white boxes indicating individual hallmark scores corresponding to points and red arrows in grey boxes indicating total hallmark scores corresponding to $P_{PROLIFERATIVE}$. TP53, tumour protein 53; CD45, cluster of differentiation 45; PCNA, proliferating cell nuclear antigen; TUNEL, terminal deoxynucleotidyl nick-end labelling; FVIII, anti-hemophilic factor; NF1, neurofibromatosis 1; PD-1, programmed cell death-1; $LADERS_{CLIN}$, clinical LUAD death score; $LADERS_{IMM}$, immunophenotypic score..